AGU PUBLICATIONS

JGR

Journal of Geophysical Research: Planets

RESEARCH ARTICLE
10.1002/2016JE005163

Key Points:
- Olivine and Fe/Mg phyllosilicates are common in Gale rim/wall rocks; feldspar-rich units were searched for but not detected
- Multiple units with hydrated and hydroxylated materials are found in floor materials southwest of MSL's landing site
- A >90 m succession of finely layered sediments on the NW Gale crater floor may record changes between lacustrine and aeolian environments

Correspondence to:
J. Buz
jbuz@gps.caltech.edu

Citation:
Buz, J., B. L. Ehlmann, L. Pan, and J. P. Grotzinger (2017), Mineralogy and stratigraphy of the Gale crater rim, wall, and floor units, *J. Geophys. Res. Planets*, *122*, 1090–1118, doi:10.1002/2016JE005163.

Received 1 SEP 2016
Accepted 17 APR 2017
Accepted article online 20 APR 2017
Published online 30 MAY 2017

Mineralogy and stratigraphy of the Gale crater rim, wall, and floor units

Jennifer Buz[1], Bethany L. Ehlmann[1,2], Lu Pan[1], and John P. Grotzinger[1]

[1]Division of Geological and Planetary Sciences, California Institute of Technology, Pasadena, California, USA, [2]Jet Propulsion Laboratory, California Institute of Technology, Pasadena, California, USA

Abstract The Curiosity rover has detected diverse lithologies in float rocks and sedimentary units on the Gale crater floor, interpreted to have been transported from the rim. To understand their provenance, we examine the mineralogy and geology of Gale's rim, walls, and floor, using high-resolution imagery and infrared spectra. While no significant differences in bedrock spectral properties were observed within most Thermal Emission Imaging System and Compact Reconnaissance Imaging Spectrometer for Mars (CRISM) scenes, some CRISM scenes of rim and wall rocks showed olivine-bearing bedrock accompanied by Fe/Mg phyllosilicates. Hydrated materials with 2.48 μm absorptions in Gale's eastern walls are spectrally similar to the sulfate unit in Mount Sharp (Aeolis Mons). Sedimentary strata on the Gale floor southwest of the landing site, likely coeval with the Bradbury units explored by Curiosity, also are hydrated and/or have Fe/Mg phyllosilicates. Spectral properties of these phyllosilicates differ from the Al-substituted nontronite detected by CRISM in Mount Sharp, suggesting formation by fluids of different composition. Geologic mapping of the crater floor shows that the hydrated or hydroxylated materials are typically overlain by spectrally undistinctive, erosionally resistant, cliff-forming units. Additionally, a 4 km impact crater exposes >250 m of the Gale floor, including finely layered units. No basement rocks are exposed, thus indicating sedimentary deposits ≥250 m beneath strata studied by Curiosity. Collectively, the data indicate substantial sedimentary infill of Gale crater, including some materials derived from the crater rim. Lowermost thin layers are consistent with deposition in a lacustrine environment; interbedded hydrated/hydroxylated units may signify changing environmental conditions, perhaps in a drying or episodically dry lake bed.

Plain Language Summary The Curiosity rover has detected diverse rocks on the floor of Gale crater; these are interpreted to have been transported there from the crater rim. To better constrain where these rocks came from, we examine the mineralogy and geology of Gale's rim, walls, and floor, using high-resolution images and spectra. While the majority of Gale is dusty and did not reveal any convincing mineral signatures, we did observe some portions of the rim and wall showing iron-rich minerals and probable iron or magnesium bearing clays. Rocks on the Gale floor also have hydration signatures similar to those of clays. These clays and those from the rim and wall are different from those in Mount Sharp because they do not have aluminum; this suggests that the waters they formed in or the rocks they came from were different. Geologic mapping of the crater floor shows that the clay-like materials are typically overlain by bland-appearing, erosionally resistant, cliff-forming units. Additionally, a 4 km impact crater exposes >250 m of material below the Gale floor, including rocks that appear finely layered. None of the original crater rocks are exposed, only rocks that later filled Gale. This indicates later deposits ≥50 m beneath those traversed by the Curiosity rover. Collectively, the data indicate substantial infill of Gale crater, including materials derived from the crater rim. The lowermost thin layers are consistent with deposition in a lake; alternating levels of hydration in the mapped rock units may imply changing environmental conditions, perhaps in a drying or episodically dry lake bed.

1. Introduction

The Mars Science Laboratory (MSL) was sent to Gale crater with a goal of assessing past habitability in the region. Gale crater was selected primarily because of a large interior central mound, Aeolis Mons, informally known as Mount Sharp, made of roughly flat-lying strata which may preserve evidence for sequential changes in the Martian environment [*Grotzinger et al.*, 2012]. Previous remote sensing studies of Gale crater have focused on the formation of Mount Sharp by exploring its geomorphology, thermophysical properties, and mineralogy [*Malin and Edgett*, 2000; *Pelkey and Jakosky*, 2002; *Pelkey et al.*, 2004; *Rogers and Bandfield*, 2009; *Anderson and Bell*, 2010; *Milliken et al.*, 2010; *Thomson et al.*, 2011; *Grotzinger et al.*, 2012; *Fraeman et al.*, 2013; *Kite et al.*, 2013a; 2013b; *Le Deit et al.*, 2013; *Wray*, 2013; *Milliken et al.*, 2014; *Fraeman et al.*, 2016].

In these works, a wide range of hypotheses have been proposed to explain the Mount Sharp sedimentary rocks, including formation by deposition in a lacustrine environment, aeolian deposition, fluvial deposition, ice-mediated air fall deposition, ashfall, or some combination of these processes. Curiosity rover data so far support only fluvial, deltaic, lacustrine, and aeolian modes of deposition for basal Mount Sharp strata of the Bradbury group, interfingering Murray formation, and unconformably overlying Stimson formation [*Grotzinger et al*., 2014, 2015; *Banham et al*., 2016]. During the first 4 years of its mission, Curiosity traversed the northern Gale floor deposits of the Bradbury group and subsequently began its ascent through strata of the underlying Mount Sharp group [*Grotzinger et al*., 2014, 2015]. Measurements taken by MSL have thus far shown that the float rocks and strata present on the floor of Gale crater host an unexpectedly wide range of lithologic compositions, including clasts of alkaline basalt and felsic igneous float rocks in strata of the Bradbury group, basaltic mudstones with Fe/Mg phyllosilicates at Yellowknife Bay, and K-feldspar-enriched sandstone at the Kimberley [*Bish et al*., 2013; *Blake et al*., 2013; *Stolper et al*., 2013; *McLennan et al*., 2014; *Sautter et al*., 2014; *Schmidt et al*., 2014; *Vaniman et al*., 2014; *Treiman et al*., 2016]. A key question centers around the source of this lithologic diversity: is it related to the bedrock of the Gale crater walls and surrounding watershed? A product of sediment sorting and chemical alteration within the crater? Or sourced from ashfall or another unknown regionally widespread geologic process?

This study builds on previous work within and around Gale crater, focusing on the wall, rim, and floor units of Gale crater. The goal is to elucidate the relationships between the bedrock materials of the wall, rim, and floor with sedimentary units traversed over and analyzed by the MSL Curiosity rover. We seek to determine the provenance for some of the unique mineralogical detections made by MSL, the relative order in which materials were deposited in Gale crater, and how they might have been altered since or during transport, as recorded in the sedimentary rocks on the floor as seen from orbit. We first provide some background on the geology, mineralogy, and chemistry of the study region. We then describe previously and newly reported detections of minerals within the Gale rim, wall, and floor rock; report the results of geologic mapping of floor units extending from the rim to the Murray formation; and summarize the observed stratigraphy of sedimentary fill in Gale crater with a focus on how the observed mineralogy and morphology of units results from changes in the paleoenvironment. Finally, we describe the implications for the source rocks and how they might have changed during transport, deposition, and as part of a changing environment within Gale, as told by the mineralogy.

2. Geologic Context

Gale is an ~150 km diameter impact crater situated along the Martian crustal dichotomy boundary. Current age estimates for the formation of Gale based on crater counting converge around 3.6–3.8 Ga, the late Noachian-Hesperian boundary [*Cabrol et al*., 1999; *Thomson et al*., 2011; *Le Deit et al*., 2013]. Reconstruction of the bedrock stratigraphy and dating by crater counting places the formation age of Mount Sharp soon after formation of the crater [*Thomson et al*., 2011; *Grant et al*., 2014; *Palucis et al*., 2016]. High-resolution imagery and spectroscopic data in the last decade have allowed further characterization of the Mount Sharp group, which comprise the lowermost exposed units of Mount Sharp [*Grotzinger et al*., 2015]. Orbital observations of this interval of strata reveal iron smectite clays, iron oxides, silica, and strong hydration signatures with distinctive strata bearing monohydrated and polyhydrated sulfates [*Pelkey et al*., 2004; *Milliken et al*., 2010; *Thomson et al*., 2011; *Fraeman et al*., 2013; *Le Deit et al*., 2013; *Fraeman et al*., 2016]. Additionally, numerous valleys and canyons have been identified that incise the Mount Sharp group strata [e.g., [*Anderson and Bell*, 2010; *Milliken et al*., 2014; *Palucis et al*., 2016]. The presence of hydrated minerals decreases while dust cover increases with elevation on the mound [*Pelkey et al*., 2004; *Le Deit et al*., 2013]. Nevertheless, boxwork structures indicating subsurface fluid flow and diagenesis are found at higher elevations [*Siebach and Grotzinger*, 2014], just beneath the unconformity that marks the top of the Mount Sharp group [*Grotzinger et al*., 2015].

Measurements taken by MSL thus far have revealed diverse chemistry and mineralogy of float rocks and exposed bedrock in the Bradbury group, the stratigraphically oldest unit explored by Curiosity [*Bish et al*., 2013; *Blake et al*., 2013; *Stolper et al*., 2013; *Sautter et al*., 2014; *Schmidt et al*., 2014; *Thompson et al*., 2015; *Treiman et al*., 2016]. The Bradbury group includes alluvial fan facies and inferred sediment transport

directions that indicate derivation from the northern crater wall and rim [*Williams et al*., 2013; *Grotzinger et al*., 2014, 2015; *Szabo et al*., 2015]. Some of the float rocks and conglomerate clasts have high alkalinity and/or abundant feldspars [*Stolper et al*., 2013; *Sautter et al*., 2014], which have not been observed from orbit. Additionally, there is high chemical variability locally within the Bradbury, such as between the Sheepbed mudstone and the Gillespie sandstone members of the Yellowknife Bay formation, which both also differ from the Bradbury rise rocks, just ~400 m away [*McLennan et al*., 2014; *Vaniman et al*., 2014]. The Sheepbed and Gillespie bulk chemistry is subalkaline basaltic, and they did not have the high feldspar composition of some Bradbury rise rocks [*McLennan et al*., 2014]. The Kimberley formation, which represents the middle part of the Bradbury group, is highly potassic, containing approximately 21% alkali feldspar by volume [*Treiman et al*., 2016]. It is hypothesized that the Kimberley formation results from the transport and mixing of sediments from two or three distinct igneous sources, perhaps from the northern Gale rim [*Treiman et al*., 2016; *Siebach et al*., 2017]. The overall diversity within the Bradbury group and the inferred diversity of its source rocks was surprising, given that orbital data of units near Gale crater showed broadly similar basaltic compositions to those near the Gusev landing site in thermal infrared and gamma ray spectrometer data [*Rogers and Christensen*, 2007; *Taylor et al*., 2010].

The regional mineralogy and chronology have been studied for the greater Gale watershed. Gale crater is at the northeast terminal extent of the Gale-Knobel-Sharp (GKS) watershed system which initiates north of Herschel crater [*Ehlmann and Buz*, 2015]. Large-scale fluvial activity last occurred in the late Noachian/early Hesperian [*Irwin et al*., 2005; *Fassett and Head*, 2008] and subsequently became increasingly more localized in the late Hesperian/early Amazonian [*Grant et al*., 2014; *Ehlmann and Buz*, 2015]. It is possible that erosion during this and subsequent times resulted in material being transported into Gale crater relatively long distances, contributing basin filling sediments [*Ehlmann and Buz*, 2015; *Palucis et al*., 2016]. Key results from study of the mineralogy with high-resolution visible/shortwave infrared data included widespread detections of olivine (sometimes with pyroxene) in the bedrock, hydrated silicates present in both bedrock and sediments, and regional or temporal differences in water chemistry as evidenced by the presence of chloride salts in the Sharp-Knobel watershed system and sulfate salts found by the rover in Gale crater [*Vaniman et al*., 2014; *Ehlmann and Buz*, 2015]. Fe/Mg phyllosilicates, kaolin family minerals, hydrated silica, and other hydrated/hydroxylated phases were detected regionally in a variety of locations including fluvial valley walls and crater rims and floors [*Wray*, 2013; *Carter et al*., 2015; *Ehlmann and Buz*, 2015]. What is not clear is whether some of the materials that may have contributed to the accumulation of Mount Sharp strata were derived from long distances in the GKS watershed versus locally within the immediate surroundings of Gale crater, including from the northern rim, the presumed source for much of the Bradbury group. We thus use remote sensing data to examine in greater detail the Gale crater basement rocks and northwestern floor rocks near the MSL landing site.

3. Methods

3.1. Mineralogy

Because we are interested in the basement bedrock and overlying floor deposits of Gale, we focused our data analysis on scenes along the Gale rim, wall, and floor, including scenes where erosion or small craters have exposed the stratigraphy of floor units. We did not analyze data over Mount Sharp as prior works have described its mineralogy [e.g., *Milliken et al*., 2010; *Fraeman et al*., 2016]. Full- and half-resolution targeted images from the Compact Reconnaissance Imaging Spectrometer for Mars (CRISM) on board the Mars Reconnaissance Orbiter (MRO) were examined. CRISM is a push broom imaging spectrometer which acquires data between 0.36 and 3.92 μm sampled at ~6.55 nm/channel [*Murchie et al*., 2007]. At highest spatial resolution CRISM is capable of resolving 15–19 m/pixel. The wavelength range and spectral resolution of CRISM allow for detection of many minerals via diagnostic absorptions including those related to electronic transitions in iron and vibrations associated with H_2O, CO_3, and metal-OH bonds [e.g., *Clark et al*. [1990]]. In total, 34 targeted images along the rim, wall, and floor of Gale crater were analyzed in this study (Figure 1). Reduced spatial and spectral resolution "mapping" products are also available from CRISM. These were used in regions where targeted CRISM scenes were not available; however, due to their lower spectral and spatial resolution and the relatively small exposures of bedrock with low dust cover, no additional mineral identifications were found using the mapping products.

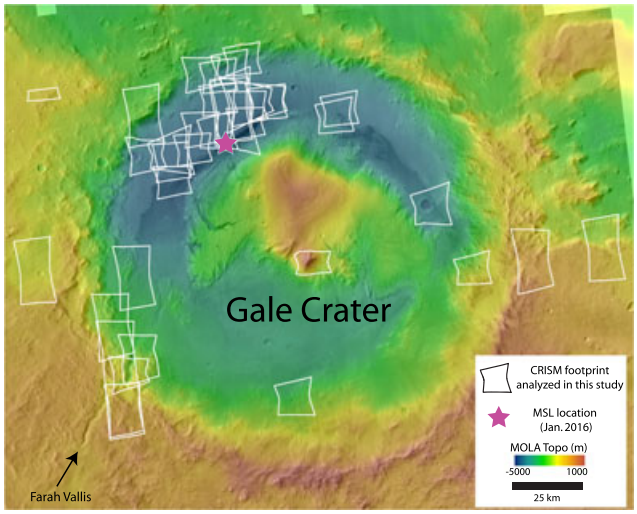

Figure 1. CRISM images analyzed in this study on a CTX mosaic with MOLA topography overlain. There is continuous CRISM coverage over the MSL landing site and traverse regions, but CRISM coverage over the remainder of Gale crater is sparser. Our study focused on all full- and half-resolution, long-wavelength CRISM scenes acquired over the walls, floor, central peak, and smaller craters within Gale (white outlines), which have the potential to reveal mineralogy of the bedrock and floor units. Those where discrete minerals were identified, enhanced above the basaltic background, are shown in Figure 2.

Standard data processing procedures were applied to the CRISM spectral cubes to calibrate and atmospherically and photometrically correct the data. These procedures include a simple cos *i* photometric correction, which assumes isotropic surface scattering, and division by a scaled atmospheric transmission spectrum, derived from a volcano scan image through the CRISM Analysis Tool toolbox [*Morgan et al*., 2009]. Because many of the CRISM scenes in this region are dusty and/or noisy [*Kreisch et al*., 2015] (see *Murchie et al*. [2009] for a review of noise sources for the CRISM detectors), a denoise algorithm was developed to further aid in mineral identification [*Pan et al*., 2015]. This algorithm excludes noisy pixels and bad spectral channels in a given image, identifies the pixels below a threshold value for several spectral parameters, and then creates "bland" spectra for use as a spectral denominator by using a column-based median of the identified bland pixels. After computing scene-derived denominator spectra for each column, the algorithm calculates the ratio spectrum of each pixel in the scene, thereby accentuating all the possible mineral detections relative to the spectrally bland regions in the same image. By ratioing a region of interest to a spectrally bland region from the same detector columns, we remove column-dependent detector artifacts and spectral signatures from materials found in common between the two areas, so the mineral signatures and spectral differences within the region of interest become more pronounced. Those spectra with possible mineral detections are then compared with the original spectra from the full-noise, unratioed data cube for validation. Additionally, after spectra of interest were acquired, absorption positions were determined using the calibrated data record wavelengths of the center pixel of each region of interest so as to properly account for the spectral smile of the CRISM instrument [*Murchie et al*., 2009]. Many unit identifications were also made through the aid of standard spectral parameter maps [*Pelkey et al*., 2007; *Wiseman et al*., 2010; *Viviano-Beck et al*., 2014].

Data from the Thermal Emission Imaging System (THEMIS) instrument on the Mars Odyssey orbiter were also used to examine the composition of the Gale rim. THEMIS contains eight detectors within the 6.8 to 13.6 μm region and captures images at a spatial resolution of approximately 100 m/pixel [*Christensen et al*., 2004]. CRISM is not capable of distinguishing iron-free high-Si silicates because the characteristic vibrations from the SiO_2 molecule occur at longer wavelengths than those sensed. In contrast, the THEMIS band passes are suited for the examination of the Si-O stretch spectral region, permitting distinctions of mafic and felsic lithologies and variability in constituent materials within these. In order to contrast and identify regions with different silicate compositions, which may be particularly mafic or felsic, we computed decorrelation stretches (DCSs) using THEMIS data following *Christensen et al.* [2005]. DCSs enhance color separation and help identify specific geologic units, which appear as different colors correlated with different surface properties in the DCS product. A DCS stretch with THEMIS bands 8, 7, and 5 (R, G, and B, respectively) aids in discrimination of Thermal Emission Spectrometer Types 1 and 2 surfaces [*Bandfield et al*., 2000] and has been used to identify mafic materials which appear pink/magenta [e.g., *Rogers et al*., 2005; *Rogers and Fergason*, 2011] and chloride-bearing materials which appear blue [e.g., *Osterloo et al*., 2010]. DCS 6/4/2 can highlight regions containing high bulk silica [*Bandfield et al*., 2013] in magenta colors and can also indicate differences in surface roughness and gray body emissivity [*Bandfield*, 2009].

3.2. Stratigraphy and Geologic Mapping

Following the identification of mineralogical/compositional units, we examined the morphology of exposures and mapped the distinct compositions identified to surface morphology, delineated using high-resolution image data. For mapping and stratigraphic studies we used imagery from the Context Camera (CTX) [*Malin et al*., 2007] and High Resolution Imaging Science Experiment (HiRISE) [*McEwen et al*., 2007] instruments, both on MRO. We constructed a full-coverage CTX mosaic over the Gale region, using images acquired in gray scale visible at a resolution of ~6 m/pixel and in swaths ~30 km wide. At select locations, HiRISE data were available with a resolution ~30 cm/pixel in ~6 km wide long swaths. We also incorporated topographic data from the Mars Orbiter Laser Altimeter (MOLA) instrument and CTX and HiRISE stereo pairs, including red-blue anaglyphs and processed digital elevation models (DEMs), either made as part of this study (using the Ames stereo pipeline) or available as HiRISE team products. We traced unit boundaries where differences in color, albedo, morphology, and texture were apparent. For example, dark, cliff-forming units with high crater retention were separated from light-toned hummocky units with few craters. We were sometimes also able to distinguish geologic units based on differences in mineralogy seen with CRISM observations, e.g., phyllosilicate-bearing units versus spectrally bland units.

4. Results

In the subsequent section, we describe the minerals detected on the rim, wall, and floor of Gale with CRISM and THEMIS (section 4.1). Section 4.2 gives the context for each detection including the location and material type for each unit (e.g., crater ejecta, bedrock, and valley wall). Section 4.3 details the results of geologic mapping, describing the discrete units on the NW crater floor (near the MSL rover) and the stratigraphy determined from topographic data and via direct observations of layering observed in a crater on the Gale floor.

4.1. Mineral Detections

4.1.1. CRISM

Minerals were identified with CRISM in a variety of geologic contexts including as parts of crater ejecta, on valley and crater walls, on ridges, in mass wasting deposits, and beneath cliff-forming units. In common in all of the scenes where minerals were identified, the spectral signatures were mostly present in darker or topographically rougher areas, which are presumably less covered by dust due to recent excavation or high erosion rates. Dust cover of greater than ~100 μm thickness can obscure the composition of the underlying surface lithology as sensed in visible/infrared data. As observed in prior CRISM analyses, Gale crater is very dusty [*Poulet et al*., 2014], and therefore, it is not surprising that mineral detections were only made in 10 of the 34 analyzed CRISM scenes (Figure 2).

We observed broad 1 μm absorptions in several locations in the rim and wall rocks, with band centers and widths indicative of the presence of olivine (Figure 3). The broad 1 μm absorption of olivine is the result of three overlapping electronic transition absorptions, which change systematically in position and/or strength with iron content and grain size [*Sunshine and Pieters*, 1998]. Olivine is detected in the rim bedrock in a small knob in C95A on the western wall (CRISM images will be referred to with the image type prefix and leading zeroes removed) as well as within the incised walls of Farah Vallis to the southwest. Additional non-bedrock detections occur on the walls and within or associated with smaller craters (discussed further in section 4.2). Though OMEGA data show pyroxene absorptions, associated with the southern rim of Gale [*Anderson and Bell*, 2010], the broad 2 μm feature characteristic of pyroxenes is absent or weak in both ratioed and unratioed CRISM scenes of the Gale rim. This is consistent with work in the greater Gale region where olivine is the dominant mafic signature with pyroxene accompanying it in some but not all CRISM scenes [*Ehlmann and Buz*, 2015]. An exception to the lack of pyroxene is within sand dunes on the Gale crater floor, where pyroxene absorptions are variably strong, consistent with previous studies [*Lane and Christensen*, 2013; *Seelos et al*., 2014; *Lapotre et al*., 2017]; however, we do not focus on the dunes in this study.

Absorption features associated with hydrated and hydroxylated minerals are relatively widespread, detected in nine localities (Figures 2 and 4). The phase detected is most commonly Fe/Mg phyllosilicate, though not all OH/H_2O-bearing minerals detected are Fe/Mg phyllosilicates. Some locations examined exhibit absorptions from both hydration and hydroxylation, consistent with Fe/Mg smectite clays. Other locations only exhibit absorptions associated with metal-OH vibrations (near ~2.3 μm and ~1.4 μm); still other locations only exhibit 1.9 μm vibrational absorptions due to the H_2O molecule in the mineral

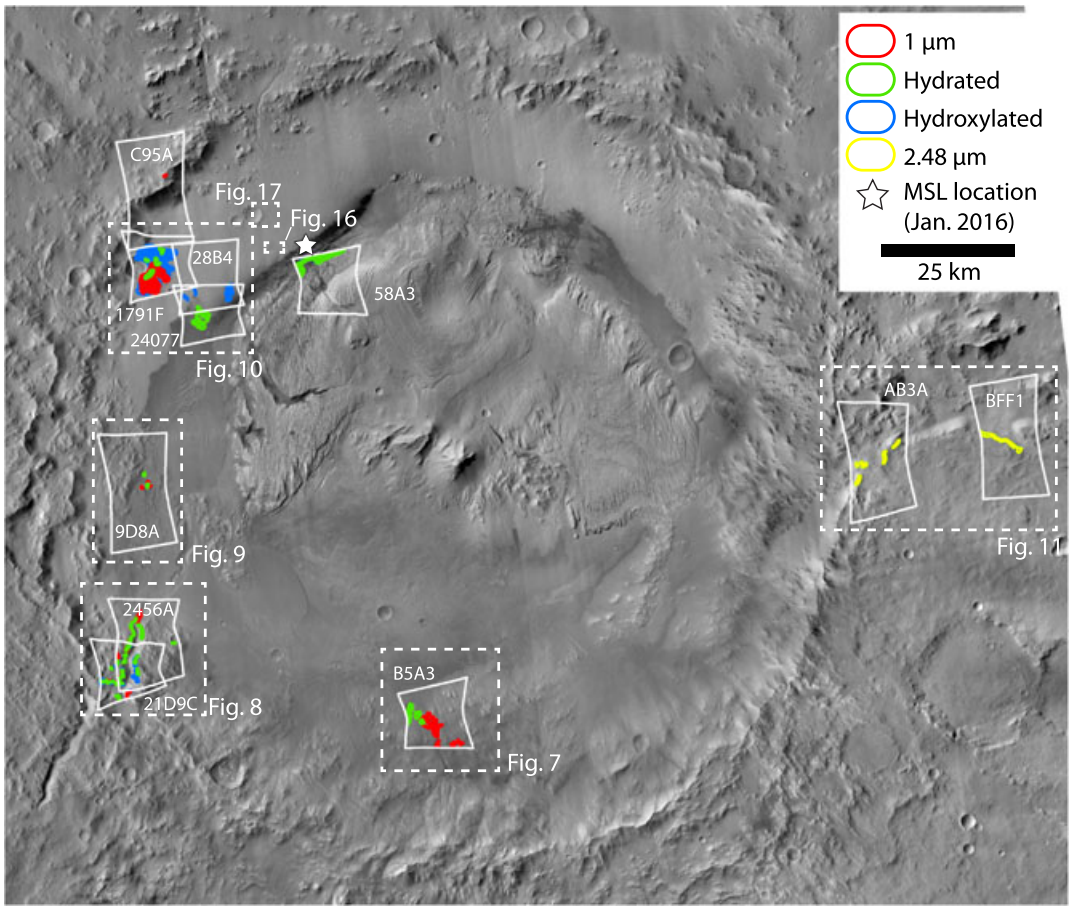

Figure 2. Regions where mineralogical absorption features are detected in CRISM images are outlined atop a CTX mosaic. Although CRISM coverage of Gale is extensive (Figure 1), the outlined scenes are the only scenes in which mineral absorptions were found above background. Olivine is indicated by an absorption centered near 1 μm. Other minerals range in hydration state, some only exhibiting an H_2O absorption at 1.9 μm (hydrated, green), others exhibiting metal-OH vibrational features at 2.3 and/or 1.4 μm (hydroxylated, blue), and some showing all three absorptions. Hydrated materials with a 2.48 μm absorption were found east of Gale (yellow). Some of the layers within Mount Sharp also contain hydrated minerals; one example is the units within CRISM scene 58A3.

structure (Figure 4). In the 1.4 μm range both H_2O and metal-OH absorptions can cooccur. The exact wavelengths of the absorptions are determined by the metal octahedral cations present in the mineral, which can be detected and discriminated in Martian spectra of Fe/Mg phyllosilicate-bearing terrains [*Bishop et al*., 2002; 2008; *Ehlmann et al*., 2009; *Michalski et al*., 2015], including within the Gale region. Many of the detections with metal-OH absorptions present have a 2.3 μm absorption which lies intermediate to the band centers observed for Fe and Mg smectites (Figure 4c; see also section 5.1). These spectra are also distinct from the stratigraphic layer containing nontronite in Mount Sharp identified by *Milliken et al*. [2014], as previously reported for a few select locales [*Ehlmann and Buz*, 2015]. The Mount Sharp spectra are most similar to Al-substituted nontronite due to the absorption shoulder at ~2.24 μm, an Al,Fe-OH vibration [*Milliken et al*., 2010]. None of the wall, rim, or floor detections have such a pronounced shoulder, although some may have a subtle signature at this wavelength such as scenes 2456A and 21D9C (Figure 4).

On the eastern rim of Gale crater and nearby bedrock exposures, two CRISM scenes reveal a new discovery: H_2O-bearing materials (as evidenced by a strong 1.9 μm absorption) which sometimes possess a broad absorption at ~2.48 μm (Figure 5). The relative strengths of the 2.48 μm and 1.9 μm features vary within the scenes. The strength of the 2.48 μm feature typically decreases when the strength of the 1.9 μm feature increases. The 2.48 μm absorption is not characteristic of one mineral in particular but may be due to

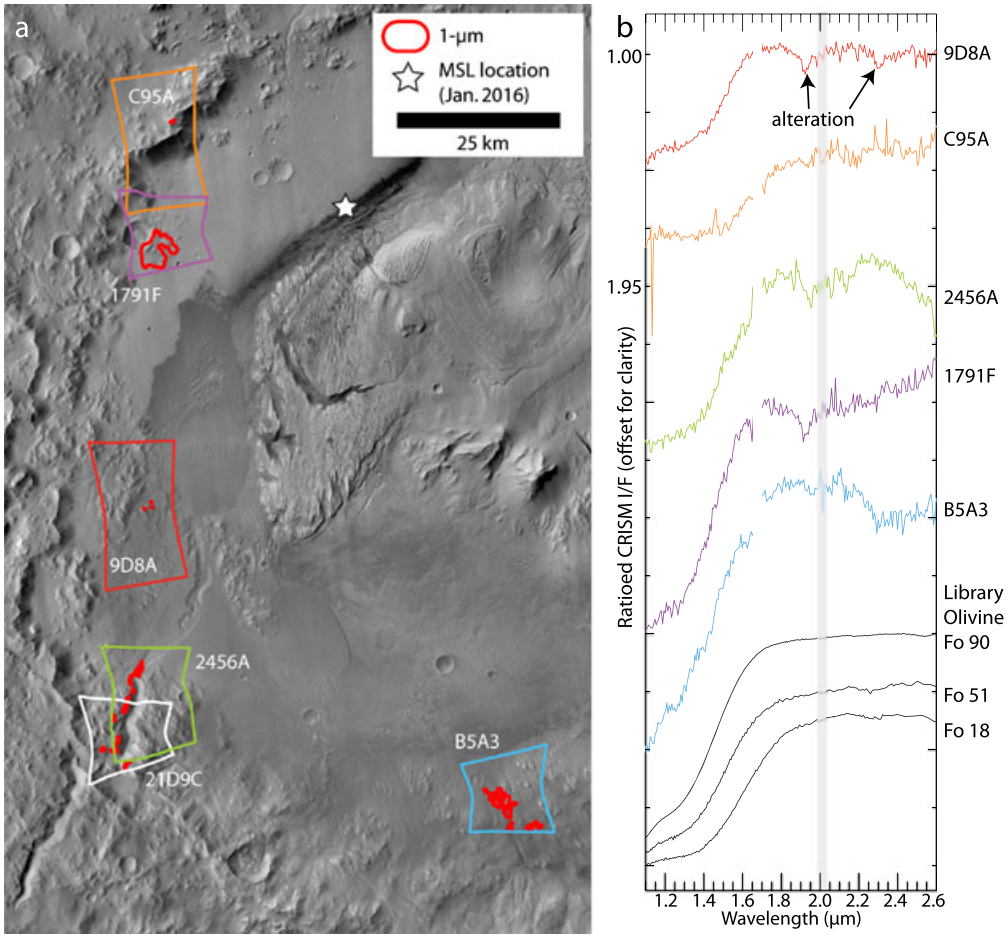

Figure 3. (a) Olivine-bearing materials are observed in the wall and rim of Gale crater with CRISM-detected locations mapped on a CTX mosaic. In CRISM scene B5A3 the 1 μm absorption is particularly strong and widespread. In scenes 2456A and 21D9C the detections are in small exposures along the top of the carved channel. Very small areas with mafic detections are also present in scenes 9D8A and C95A. (b) A broad absorption feature at 1 μm is due to electronic transitions of iron in the olivine structure. The olivine detected in CRISM scene 9D8A also has absorptions, indicating the presence of a phyllosilicate mineral, either from spatially mixed phyllosilicate-bearing materials or alteration of the olivine. Fo51 and Fo18 spectra are from *Clark et al.* [2007], and the Fo90 spectrum is from *Sunshine and Pieters* [1998].

H_2O in a mineral structure [e.g., *Clark et al.*, 1990]. We compared the CRISM spectra to a number of sulfate, zeolite, and akaganeite spectra because these minerals all have absorptions in this wavelength range. Akaganeite has been detected in nearby Sharp crater to the west [*Carter et al.*, 2015], while monohydrated and polyhydrated sulfates have been detected in Gale crater sedimentary rocks visited by Curiosity (though in low bulk abundance [e.g., *Vaniman et al.* [2014]) and within the Mount Sharp group from orbit [*Milliken et al.*, 2010; *Fraeman et al.*, 2016]. The wavelength position observed is most similar to bassanite, $CaSO_4{\cdot}0.5H_2O$, though the band centers in the 1.9 μm and 2.4 μm region could belong to a zeolite as well (Figure 5c). Though of generally similar spectral shape and with absorptions at a similar wavelength range, the absorptions appear at a slightly longer wavelength when compared with the Mount Sharp sulfates from *Fraeman et al.* [2016]. Ultimately, we are not able to definitively assign a unique mineral identification to this hydrated phase as the band centers are not at a wavelength diagnostic of one particular mineral.

The characteristic 2.2 μm feature of hydrated silica or Al phyllosilicates has been found elsewhere on the Gale crater floor [*Seelos et al.*, 2014], in the Murray formation [*Milliken et al.*, 2010; *Fraeman et al.*, 2016], and in the watershed [*Ehlmann and Buz*, 2015]. Its presence in the analyzed scenes in this study is rare to absent; some scenes (2456A and 1791F) may show it subtly at about the level of noise in the data (Figure 4).

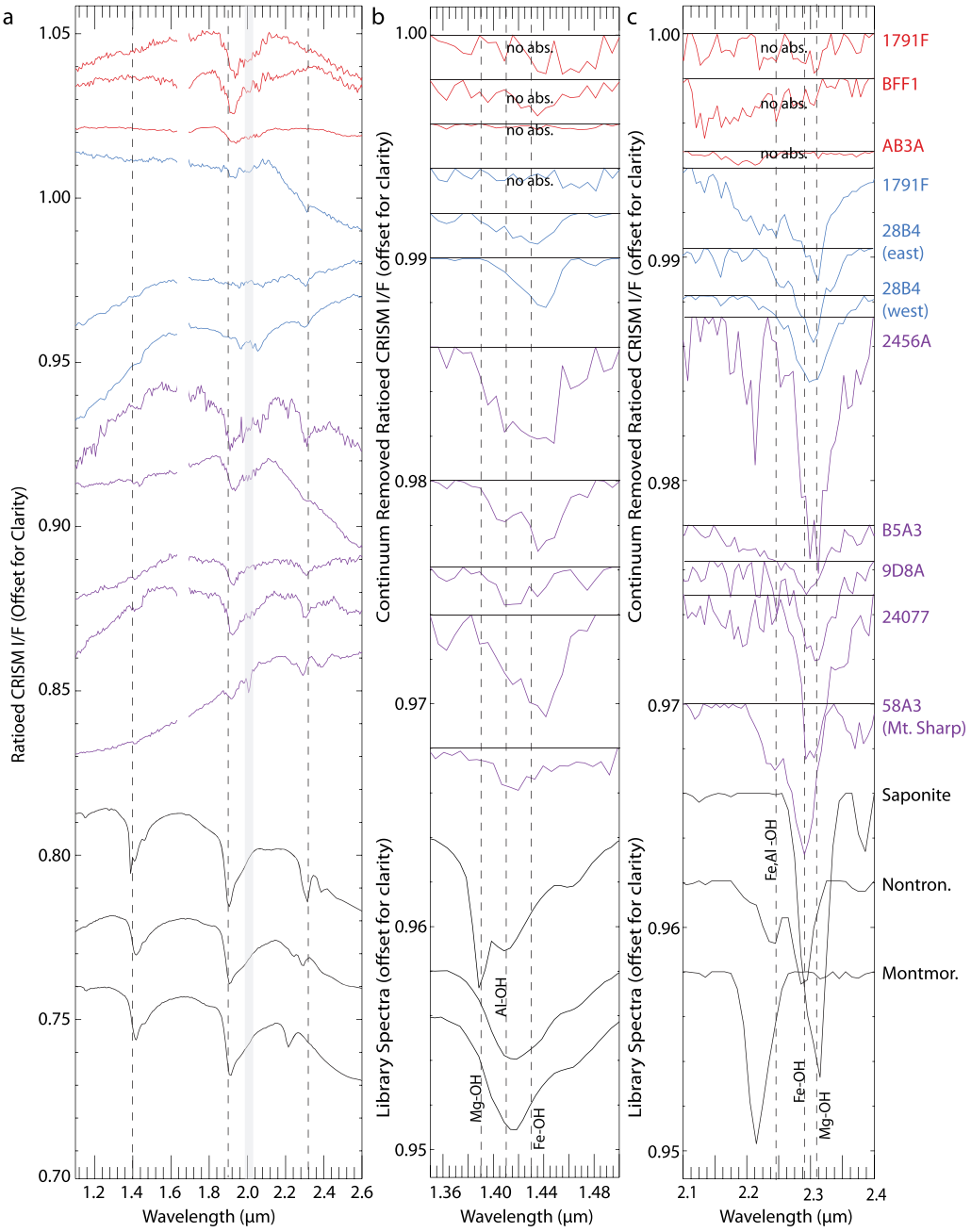

Figure 4. (a) CRISM mineral detections compared to library spectra from *Clark et al.* [2007]. Some noise removal code processed spectra of hydrated/hydroxylated materials only exhibit the H_2O absorption at 1.9 μm (red), while others exhibit only hydroxylation absorptions at 1.4 and/or 2.3 μm (blue) that permit the phase(s) present to be identified. There are also several materials that exhibit both hydration and hydroxylation (purple). Wavelengths used for the CRISM spectra are extracted from ancillary data so as to account for the detector-dependent spectral smile. (b and c) The CRISM spectra are compared to library spectra of phyllosilicate minerals after applying a linear continuum removal over the absorption. The 1.4 and 2.3 μm band positions vary according to the metal ions present in the mineral. Interestingly, absorptions in materials from the wall and rim rocks are typically at longer wavelengths than Mount Sharp nontronite spectra or library nontronite spectra. Additionally, the 58A3 spectrum from Mount Sharp also shows a shoulder near 2.24 μm characteristic of Fe,Al-OH which is not present in most spectra from other locations within Gale.

Overall, the Gale rim, wall, and floor have mineralogy similar to what has been detected in the greater Gale region [*Ehlmann and Buz*, 2015]. It appears predominantly mafic with the presence of Fe/Mg phyllosilicates. The phyllosilicate absorption detections are similar between the walls and floor but distinct from Mount

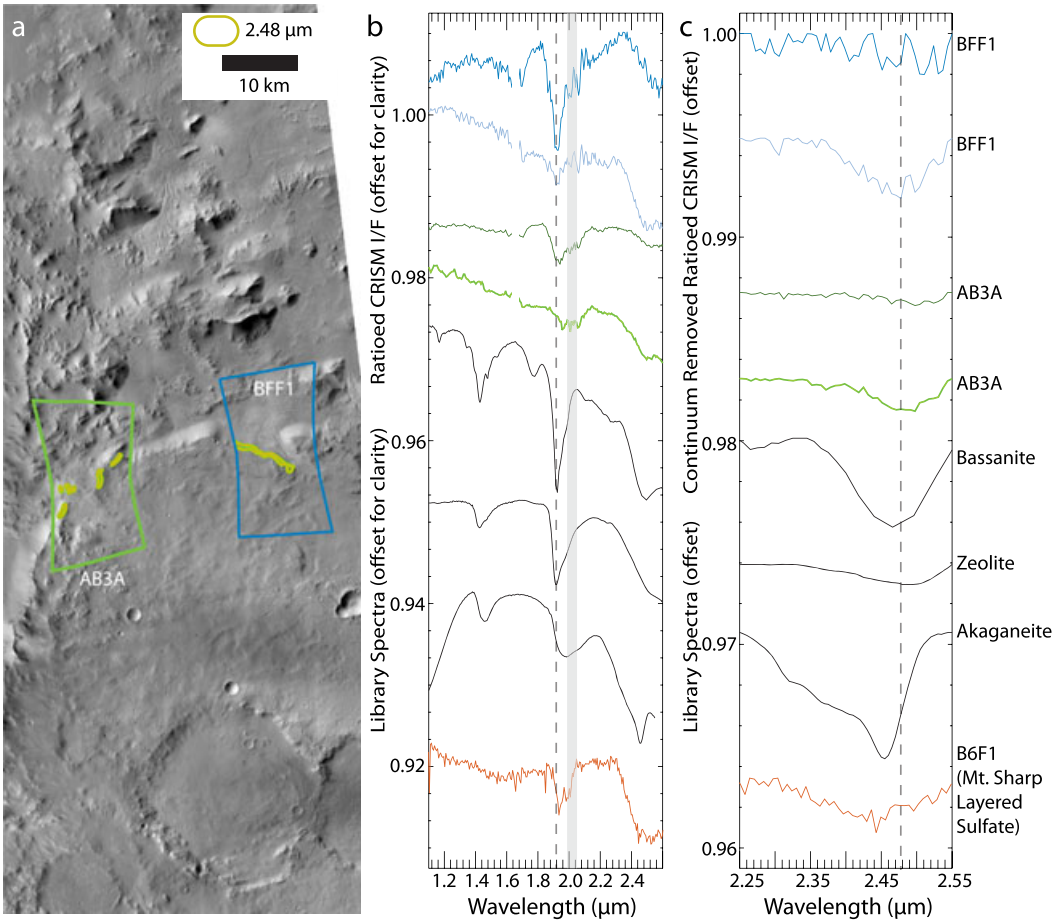

Figure 5. (a) Eastern Gale CRISM scenes AB3A and BFF1 show distinct absorptions in the 2.48 μm region not found elsewhere in Gale. These absorptions, mapped on a CTX mosaic, are localized to the plateaus on a valley that cuts through the eastern Gale rim. (b) CRISM spectra from scenes AB3A and BFF1 compared with library spectra of bassanite [*Clark et al.*, 2007], zeolite (chabazite, CRISM spectral library sample LAZE17), and akaganeite [*Bishop et al.*, 2015], as well as the layered sulfates from Mount Sharp from *Fraeman et al.* [2016]. A 1.9 μm feature is found in the regions with the 2.48 μm absorption. Materials with the strongest 2.48 μm absorption have weaker 1.9 μm absorptions. The grayed out wavelengths indicate a spectral region affected by residual atmospheric absorptions. (c) Linear continuum removal in the 2.48 μm region shows that the absorption is not uniquely characteristic of one single mineral when compared to library spectra.

Sharp [*Milliken et al.*, 2010]. Hydrated minerals, possibly similar to sulfates detected within Mount Sharp [*Fraeman et al.*, 2016], may also be present on the eastern Gale rim. No other hydrated/hydroxylated phases were identified, and iron-bearing feldspar is not found in the CRISM data.

4.1.2. THEMIS

The THEMIS DCS technique did not highlight large regions of distinctive silicate composition on the Gale rim or wall (Figure 6), e.g., from lithologies significantly enriched in feldspars. The most pronounced units in the DCS mosaics are of the active sand dunes, which in both stretch combinations show their enhancement in mafic phases, an expected result based on prior study [e.g., *Lane and Christensen*, 2013]. "Ghosting," an effect caused by band-dependent contributions from stray light in the detector combined with small-scale surface temperature differences [*Bandfield et al.*, 2004], was also present in the scenes, in particular along the Gale rim. Ghosting appears as color variation within the DCS, downtrack from features with temperature variability. The 8/7/5 DCS did, however, reveal small pink regions on the Gale rim and floor with potential olivine (Figure 6). Some of these regions corresponded to regions previously identified to have broad 1 μm absorptions through low-resolution CRISM mapping products but are not yet covered by CRISM targeted images.

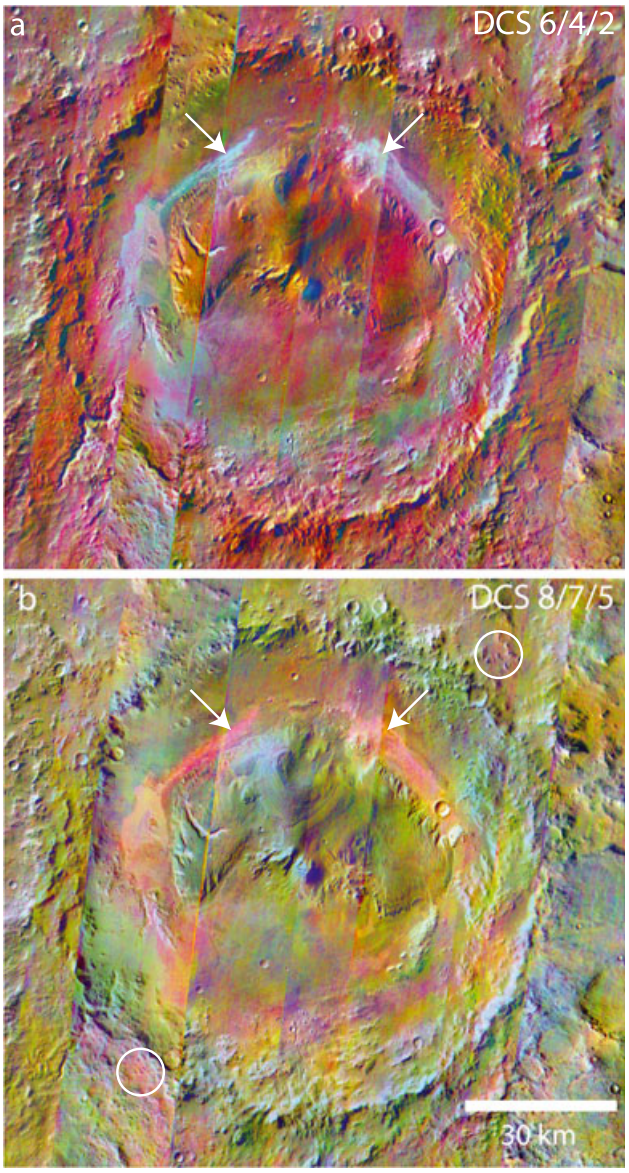

Figure 6. THEMIS DCS mosaics over the study area. (a) Mosaic of DCS 6/4/2 (R/G/B) which highlights the sand dunes at the base of Mount Sharp in cyan. The majority of the scene is red/pink, and the rim and wall do not demonstrate significant heterogeneity aside from ghosting artifacts. (b) Mosaic of DCS 8/7/5. Magenta/pink hues on part of the crater floor may indicate mafic mineralogies. The basaltic sand dunes are highlighted most prominently (indicated by arrows). Subtle pink regions (circled) in the rim correspond to a broad 1 μm absorption in CRISM mapping products.

4.2. Geologic Settings of Mineral Detections

Here we describe the morphologic characteristics of areas in which the spectroscopic detections are made, as seen in HiRISE and CTX data, in order to determine the setting of each detection and describe their occurrence/extent.

4.2.1. Southern Gale Wall

CRISM image B5A3 with detected olivine and Fe/Mg phyllosilicates is situated on the sloping southern wall of Gale crater, 15 km downslope from the rim (Figure 7; see Figure 1 for MOLA topography). The gentle slope (~7°) of this region in comparison to the steeper slopes seen in northern Gale (~12°) may indicate that there is mantling material atop the crater bedrock wall. A fluvial channel roughly bisects B5A3 and terminates just prior to a set of sand dunes at the base of the southern wall (Figure 7). Olivine is present throughout most of the scene, but olivine-related absorptions are enhanced in certain locales. Localized, more pronounced olivine signatures are seen in the southeastern corner of the CRISM scene, associated with small craters. In the middle of the scene, a 1.5 km crater and its ejecta show enhanced olivine and Fe/Mg phyllosilicates (previously reported by *Wray* [2013]). A sharply ridged downslope deposit enters another crater and probably represents a landslide of materials derived from higher up on the Gale wall (Figures 7b and 7c). The landslide has been mantled by a thin smooth layer of material, differentially eroded along its edges and obscuring the nature of its initiation (Figures 7b and 7c). Along the ridges of the landslide deposit are materials with 1.9 μm and 2.29 μm absorptions, consistent with an Fe smectite like nontronite. There is no correlation between the mineral detections and the channel, which bisects the scene. Of all the phyllosilicate detections made in the Gale rim and wall, the location of the center of the 2.3 μm absorption of this scene best matches that of Mount Sharp, although the Fe,Al-OH shoulder is absent, thus implying little Al in octahedral sites of the clay mineral.

4.2.2. Southwestern Rim-Incised Valley (Farah Vallis)

A >40 km long valley incises the southwestern Gale rim and is known as Farah Vallis. Two CRISM scenes at the lower terminus, 2456A and 21D9C, exhibit abundant olivine and Fe/Mg phyllosilicate signatures (Figure 8). HiRISE imagery in this area shows that the margins of the valley are dark, rough-textured, and have signs

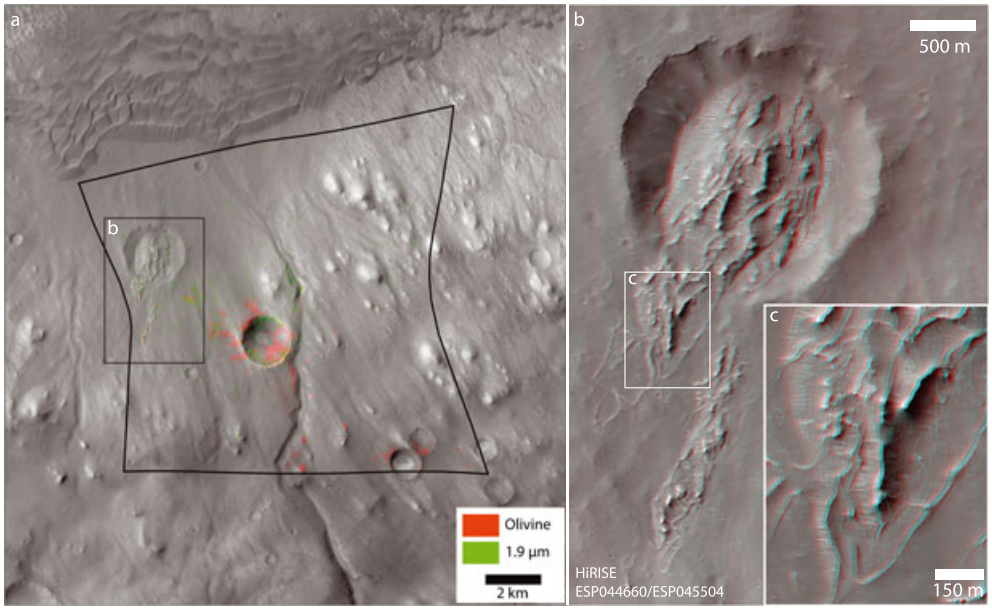

Figure 7. (a) CRISM scene B5A3 images the southern wall of Gale crater. This wall is gently sloping, compared to the northern wall, which could mean that the Gale basement rocks in the crater rim are mantled by newer material. Olivine signatures are present in much of the scene; areas with the strongest absorptions are highlighted in red. Additional absorptions due to H_2O in minerals are present in the vicinity of the central small crater in this scene as well as within a landslide deposit. These hydrated materials are not associated with the channel dissecting the scene. (b) A landslide enters and partially fills a small crater in the northwest of this scene. (c) Zoom in of the landslide's sharp ridges which are well correlated with 1.9 μm, H_2O absorptions in CRISM data.

of active modification such as boulder trails. Olivine-related, 1 μm absorptions are strongest along the steep valley rim in light-toned material (Figure 8b), while Fe/Mg phyllosilicates are found immediately below in dark, more recessive material. An ~1 km crater has impacted along the slopes of Farah Vallis (Figure 8c). This crater has particularly strong absorptions due to Fe/Mg phyllosilicate in the rim and walls. A portion of the rim of this small crater appears to have slumped downhill (Figure 8c). Spectra shown in Figure 4 indicate the possible presence also of an Al-OH absorption near ~2.2 μm, characteristic of Al phyllosilicates like kaolinite and montmorillonite that are either spatially or intimately mixed within the CRISM pixels over the Fe/Mg phyllosilicate; the Al-OH absorption is very subtle, at about the level of the noise, if indeed present.

4.2.3. Western Gale Wall

CRISM half-resolution image 9D8A was acquired over the lower portion of the western Gale wall (see Figures 9 and 1 for MOLA topography). The northeastern corner of the scene includes olivine-bearing sand dunes. Small detections (several pixels) of altered olivine and phyllosilicate material are made along the tops of small knobs along the lower wall (Figure 9b). HiRISE scene PSP007211 shows that these detections occur on the roughest material, exposed where occasional ~1 m boulders are present (Figure 9c).

4.2.4. Northwestern Gale Wall and Floor

An ~5 km crater has impacted the approximate boundary between the Gale wall and floor. The majority of this crater and its ejecta blanket are captured in CRISM scene 1791F (Figure 10). There is heterogeneous exposure of olivine and Fe/Mg phyllosilicate-bearing materials in the crater ejecta and in its walls. The relative strengths of the H_2O and metal-OH bands are variable within the scene (two spectra, Figure 4). Although olivine is patchily found throughout the ejecta blanket, one particular southeast extending streamer has an especially pronounced spectral signature.

Half-resolution CRISM scene 28B4 captures part of the northwestern Gale floor and samples crater ejecta, sand dunes, inverted channels, and several stratigraphic units. The distal extent of the ejecta from the 1791F crater is also within this scene but here does not display any spectral features. The inverted channels are inferred from their long and branching nature seen in HiRISE/CTX and terminate in similar long and branching depressions. These channels are also spectrally bland. The sand dunes are enriched in olivine and pyroxene but are not further studied.

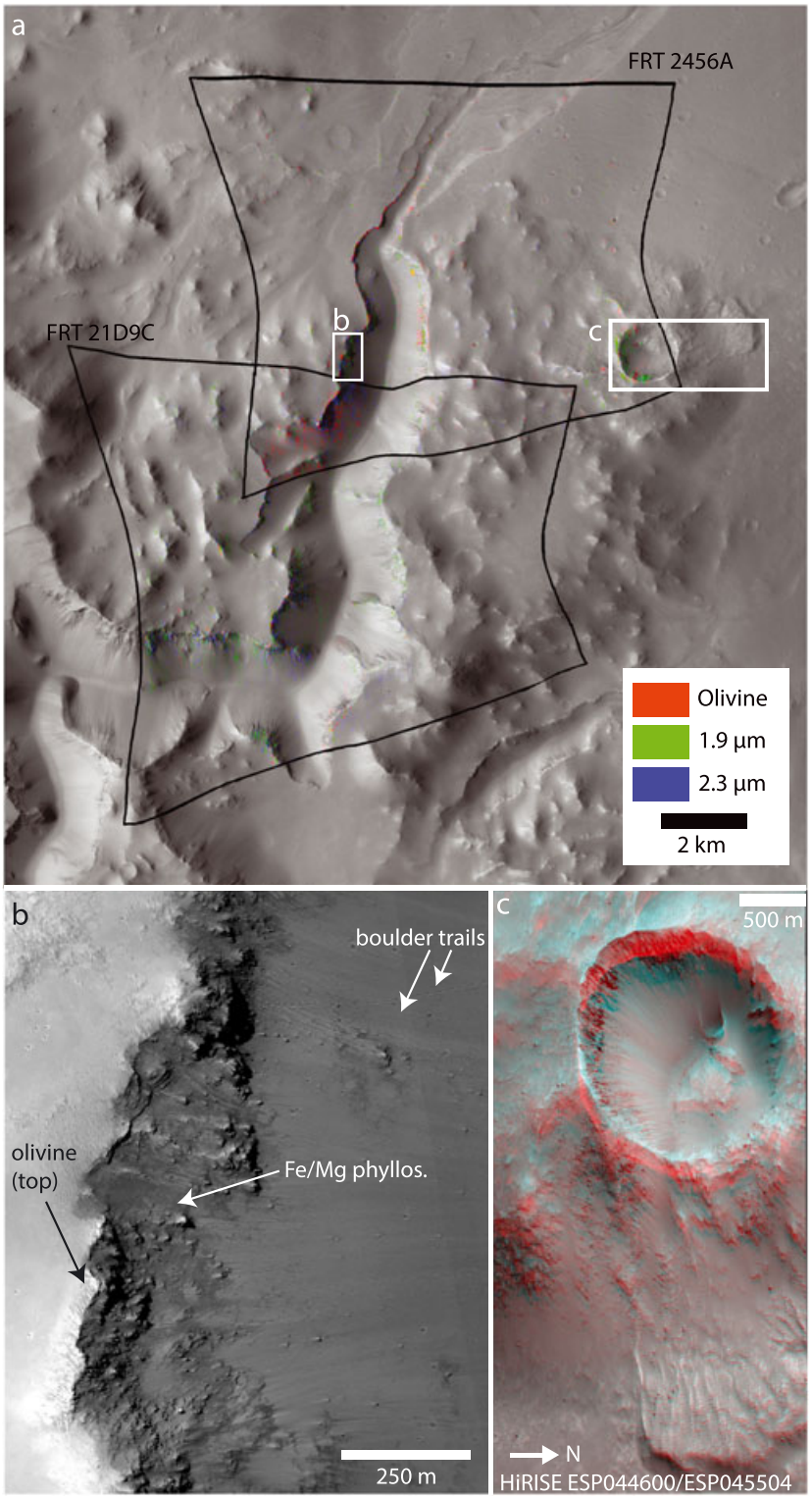

Figure 8. (a) Farah Vallis dissects Gale crater from the southwest. Fe/Mg phyllosilicates are found at the top of the valley walls as well as in a small nearby crater. A distinct, olivine-bearing unit overlies the phyllosilicates. Although in some regions of the channel, the olivine-bearing material is found coming down the channel walls, it appears to be stratigraphically above the phyllosilicates. A landslide is found to the east of the small phyllosilicate-bearing crater. (b) The channel walls are freshly exposed as evidenced by the rough textures observed, their low albedo, and boulder trails. (C) A HiRISE anaglyph (must be viewed in N-up orientation) of the small phyllosilicate-bearing crater shows that part of the crater wall appears to have slumped downhill and that the impacted material may be susceptible to mass wasting events.

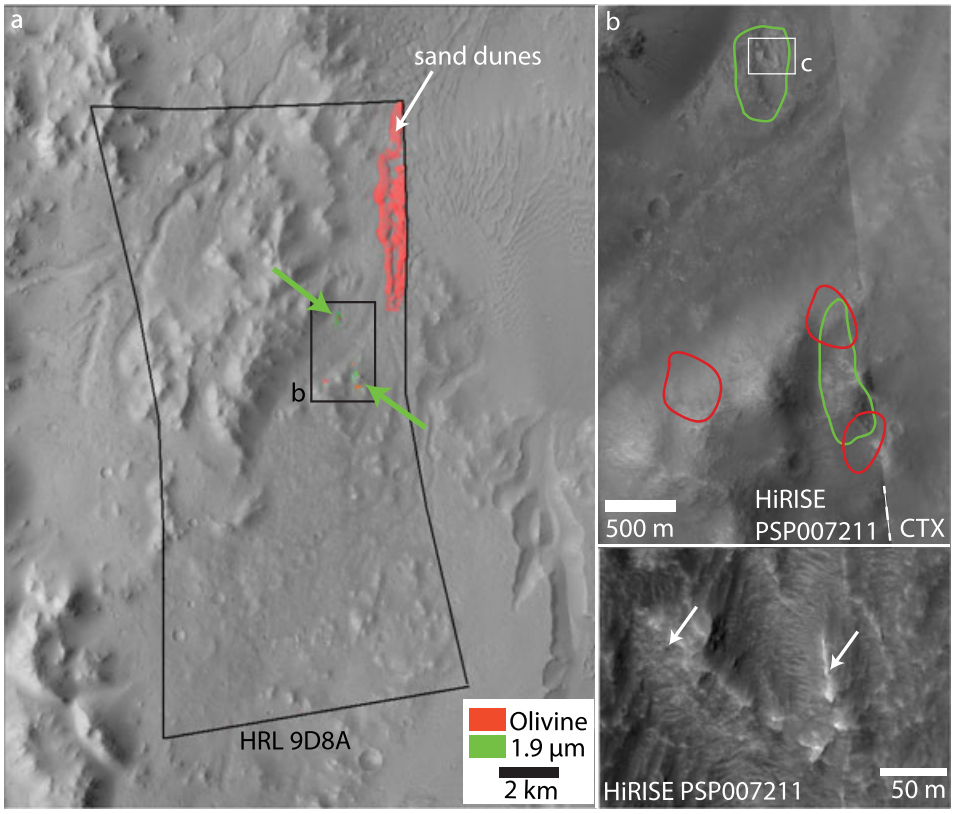

Figure 9. Small phyllosilicate occurrences on the western Gale wall. (a) Localized exposures of hydrated and mafic materials are present on the western Gale wall in CRISM scene 9D8A. (b) Using high-resolution imagery, where available, these features appear to emanate from exposed bedrock rather than filling units. (c) At the highest resolution some ~1 m boulders are apparent (indicated by the white arrows) along ridges where hydration is found. There is nothing particularly distinct about the regions where the mineral signatures are present except that they are ridges where erosion and removal of dust may facilitate CRISM detections.

The stratigraphy imaged by CRISM on the crater floor includes four units: a dark, spectrally bland cliff-forming unit, a large hummocky and partially polygonally fractured unit with associated hydroxyl-related absorptions, a hydroxylated, light-toned material visible in depressions, and a small area of ridged hydrated material, which is more extensively covered in full-resolution scene 24077 (Figure 10). The cliff-forming unit appears to overlay the other units. The hummocky material is exposed to the east of the dark cliff-forming material. HiRISE correlation with CRISM indicates that although the hummocky topography extends further, the hydroxylation is limited to a region which also bears polygonal fractures. The light-toned material is exposed to the west of the dark cliff-forming material and appears recessive and has limited exposure: it is only visible within depressions and as a layer between more competent units. The CRISM hydroxylation associated with it is similarly limited to a small area: multiple patches of several pixels each. The texture and morphology of these hydroxylated units are further discussed and imaged in section 4.3.2. The two hydroxylated units have absorption band positions at a similar wavelength in the 2.3 μm region, but the absorption positions vary slightly in the 1.4 μm region (Figure 4, "28B4 (west)" from the light-toned material and "28B4 (east)" from the polygonally fractured material). These units also have absorptions in similar position to the phyllosilicates in scenes 2456A and 9D8A (described in sections 4.2.2-4.2.3) though are missing the water absorption at 1.9 μm. The ridged material, more extensively covered in scene 24077, was previously studied by *Milliken et al*. [2014] and found to be of possible aeolian origin, inferred based on the "washboard" appearance of regularly spaced ridges, which may record large-scale cross stratification. The ridged material also contains Fe/Mg phyllosilicates, perhaps formed by diagenesis [*Milliken et al*., 2014], is spectrally distinct from the two hydroxylated units, and has polygonal fracturing on the meter scale.

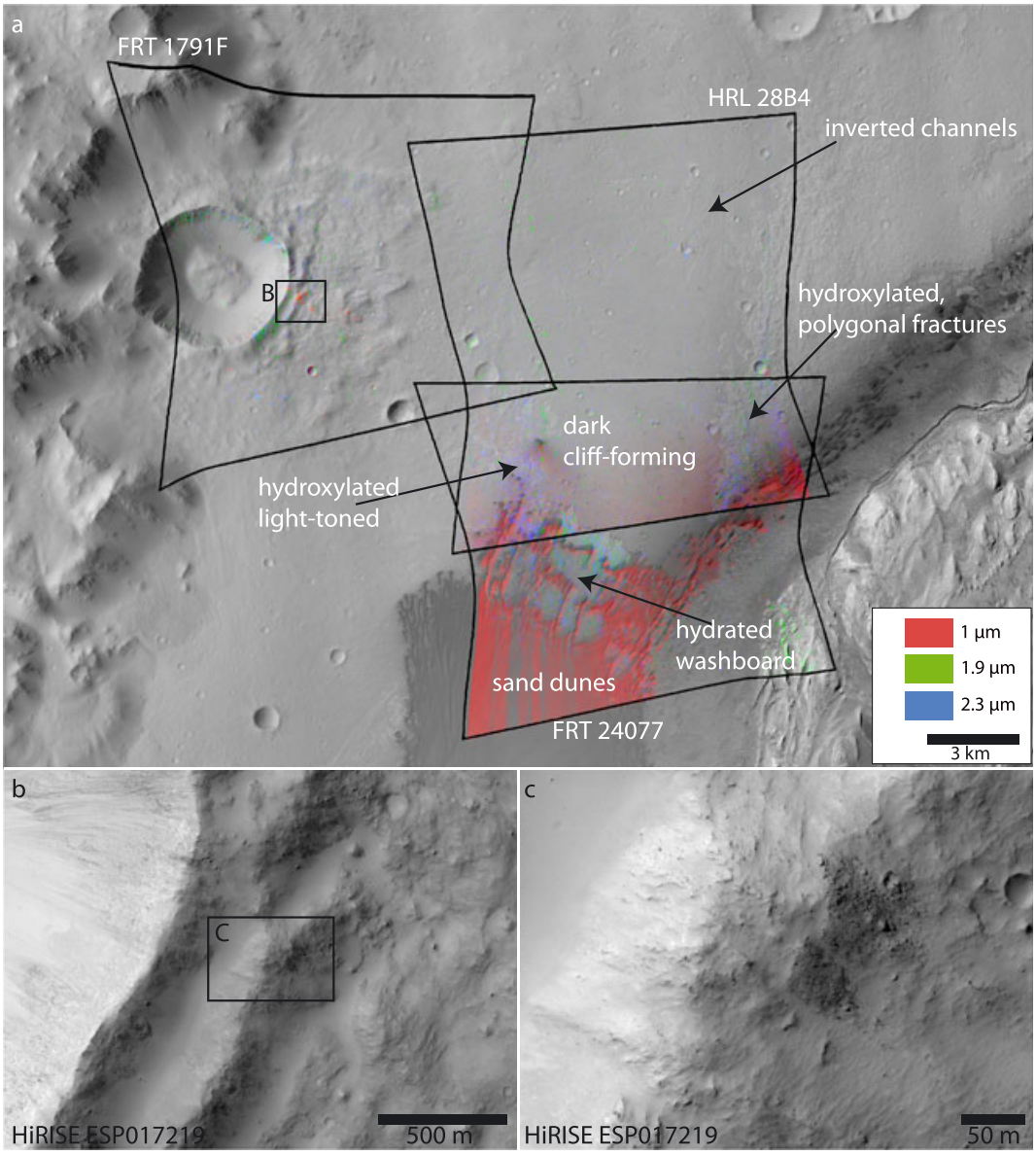

Figure 10. Mineral detections on the wall and floor in northwest Gale. (a) A 5 km diameter crater in CRISM scene 1791F has impacted Gale right at the wall/floor boundary. The crater ejecta blanket is relatively intact and exposes mafic and hydrated/hydroxylated material (previously identified by *Wray* [2013]). It is unclear if the crater is excavating Gale bedrock or later deposits, but depth-diameter scaling suggests that it may sample the Gale basement. CRISM scene 28B4 samples a dark capping unit, polygonal units on either side of this cap (which includes the fine-scale polygonal fracturing in the washboard unit), inverted channels, the edge of a previously identified washboard-textured unit [*Milliken et al.*, 2014], and sand dunes. Both of the polygonal units to the east and west of the capping unit exhibit hydroxylation. Other geologic units within the scene are spectrally bland. In scene 24077, strong hydration and hydroxylation features are seen in the washboard unit, previously identified by [*Milliken et al.*, 2014]. (b) High-resolution imagery is available in the crater ejecta. Phyllosilicates and olivine are detected patchily in the crater wall and in ridges of ejecta. (c) The strongest mafic signatures appear to be correlated with dark, rough patches of material in the crater ejecta.

4.2.5. Eastern Gale

A channel which originates from farther east breaches the eastern Gale rim (Figure 11). The north facing walls of this channel and of other nearby knobs host the hydrated material with a broad 2.48 μm absorption. These materials are not found in the debris or channel floors. HiRISE imagery indicates that some of the material is associated with boulders but otherwise the host units are not clearly defined.

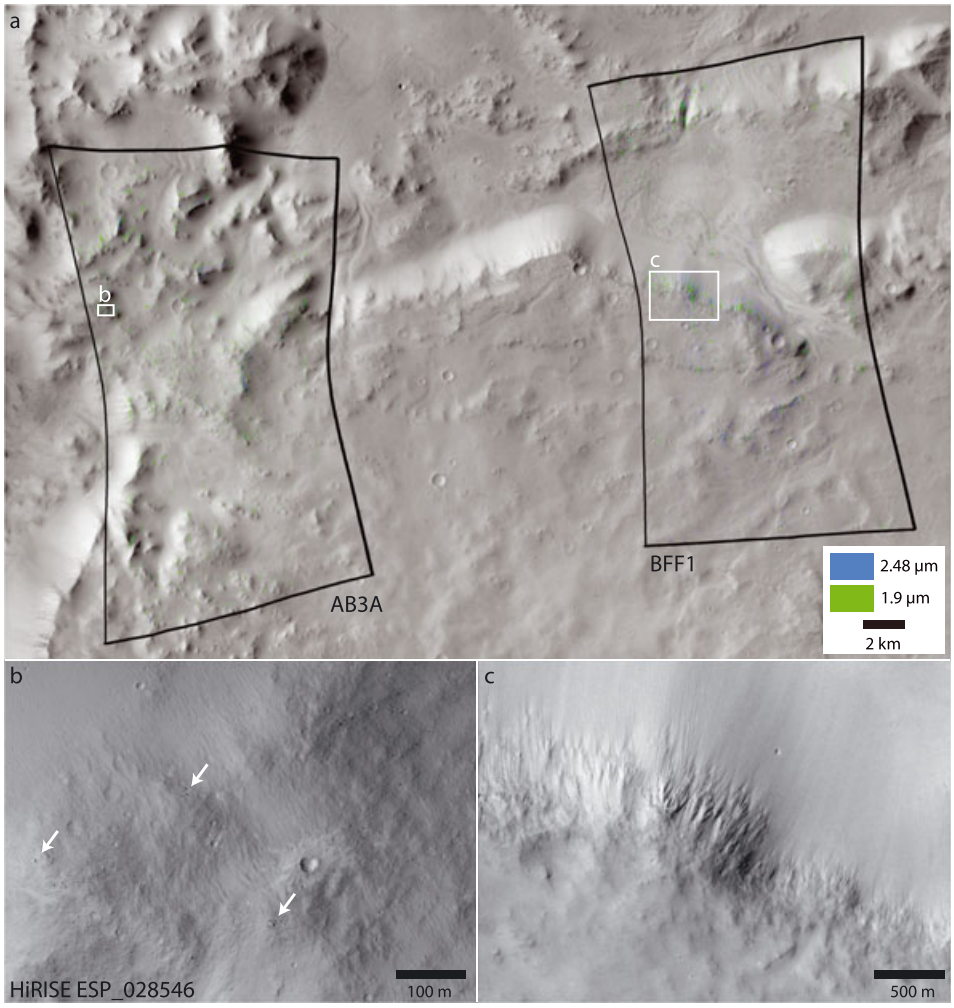

Figure 11. (a) The H_2O and 2.48 μm absorption features in AB3A and BFF1 are present along ridges and scarps in Eastern Gale, where an entering valley incised along the dichotomy boundary. (b) HiRISE imagery is available for part of CRISM scene AB3A. Highest-resolution images show that the mineral detections are associated with darker, fresh surfaces with abundant boulders (indicated by arrows). (c) The strongest detections in CRISM scene BFF1 lie along a steep slope.

4.3. Geologic Mapping and Stratigraphy of NW Gale Crater Floor

Geologic mapping of the floor of the northwestern part of Gale crater using mineralogy and morphology reveals several orbitally defined units, which we relate to stratigraphic units that have been identified by the Curiosity rover team (Figure 12) and units identified on the walls and rim of Gale. Some of the northwest Gale floor has not been mapped due to it being dusty, debris covered, and/or spectrally bland. Collectively, the surfaces and units mapped, excluding the crater-exposed stratigraphy and mass wasting surfaces, span an ~150 m elevation range observed in MOLA data (Figure 13). The mapped areas are categorized as either geomorphic surfaces or geologic units. Surfaces, described in section 4.3.1, refer to regions which have distinct boundaries (can be traced) but which do not have any stratigraphic/paleoenvironmental information (e.g., crater ejecta). Geologic units, described in section 4.3.2, refer to regions with distinct composition (from CRISM) or appearance, which may be the result of a different formation or depositional environment when compared with their surroundings (e.g., hydrated thinly layered deposits versus spectrally bland massive exposures).

Topographic and imagery data allow us to determine the stratigraphic relationships between some of the units. Additionally, within a fresh crater on the northwest floor, a series of layers is observed on the well-preserved walls. The lowest units exposed in the crater are below the elevation extent of the surfaces, landforms, and geologic units. We describe the sequence of layers observed in the crater walls and attempt to correlate it with some of the mapped floor units in section 4.3.3.

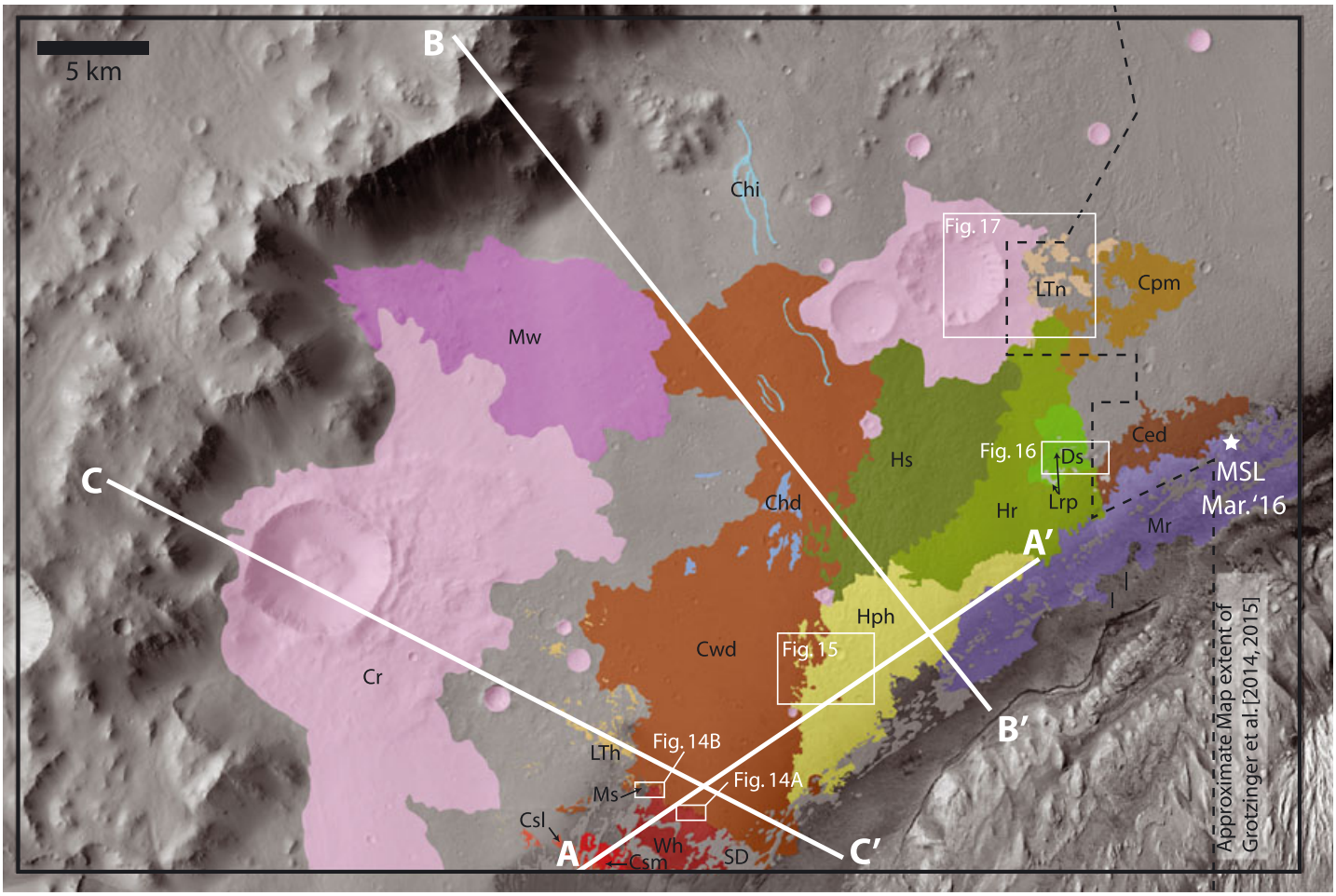

Surfaces

Cr	Crater and ejecta
Mw	Mass wasting
Chi/Chd	Channel-like: Inverted, Depressed
SD	Active Sand Dunes

Textural and Compositional Units

Cwd	Western Dark Cliff-forming
Ced	Eastern Dark Cliff-forming
Cpm	Pock-marked Cliff-forming
Csl/Csm	Smooth Cliff-forming: Light, Medium
Hs/Hr/Hph	Hummocky: Smooth, Rough, Polygonally Fract. (hydroxylated)
Lrp	Preserved linear ridges
Ds	Smooth Depression
LTn	Northern Light Toned
LTh	Hydroxylated Light Toned
Wh	Hydrated Washboard (as mapped by Milliken 2014)
Mr	Murray (as mapped by Fraeman 2016, Grotzinger 2015)
Ms	Smooth Mantling

Figure 12. (top) Geologic map of the NW Gale floor. Using imagery and mineralogical detections, we constructed a geologic map in NW Gale mapping surface landforms and geologic units. The compositional differences seen in CRISM correspond to morphological differences seen in CTX and HiRISE. The boundary for mapping done in Grotzinger [*Grotzinger et al.*, 2014, 2015] is indicated by the dashed line. By extending the geologic units drawn in previous high-resolution orbital data maps of this region, we find that Cpm and Ced are likely part of the Bradbury Group [*Grotzinger et al.*, 2014, 2015]. Topographic profiles are shown in Figure 13.

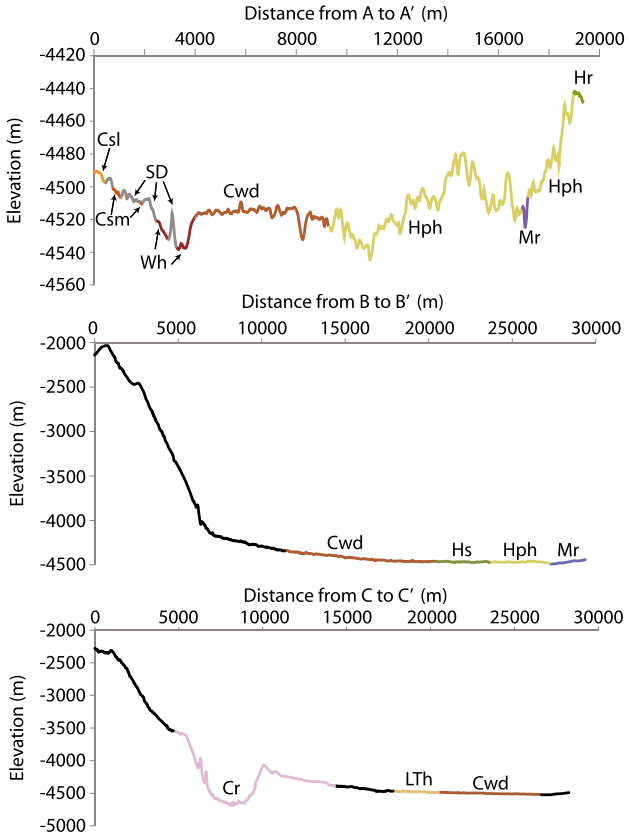

Figure 13. (top) A topographic profile crossing many of the floor units near Mount Sharp. (middle and bottom) Topographic profiles of the rim-to-crater floor transition show the generally flat nature of the Gale floor which may indicate significant sediment fill. The crater profiled in Figure 13 (bottom) demonstrates that the ejecta from this crater likely excavate both wall and floor materials.

4.3.1. Surfaces and Landforms

Surface processes such as landslides and cratering have modified the walls, rim, and floor of Gale and obscured or modified some of the geologic units. Craters and their associated ejecta blankets have been mapped together (labeled Cr). A mass wasting deposit (Mw) emanating from the northern Gale rim is also mapped. Mw is partially overlain by the ejecta of an ~7 km diameter crater, indicating Mw's older age. The Mw deposits extend approximately 7 km and terminate near their intersection with the dark competent material seen in CRISM scene 28B4 (section 4.2.4), mapped as western dark cliff-forming unit (Cwd, further described later). A series of inverted channels (Chi) can be traced from near the base of the northern Gale rim. These channels are oriented approximately in a north-south direction. The inverted channels terminate in broader channel depressions (Chd) within the limits of the cliff-forming Cwd.

4.3.2. Geologic Units

Over a dozen distinct sedimentary rock units were identified on the northwestern Gale floor. The mapping of the washboard unit (Wh) follows that of *Milliken et al.* [2010] (Figure 14). Mapping of the Murray formation follows that of *Fraeman et al.* [2016] and *Grotzinger et al.* [2015]. The remaining units are newly delineated in this work.

Multiple spectrally bland, competent, heavily cratered, resistant bedrock units were identified with distinctive morphologies that distinguish them from one another. These units are named after their cliff-forming attribute: western dark cliff-forming (Cwd), pock-marked cliff-forming (Cpm), and eastern dark cliff-forming (Ced). The cliff-forming units mapped, Cpm and Ced, correspond well with previous mapping done by the MSL team of the "rugged terrain" and "cratered surface" units, respectively [*Grotzinger et al.*, 2014]. While the Cpm pock-marked unit is somewhat localized, the Ced eastern dark unit is more extensively exposed and extends south and eastward toward the lower Mount Sharp units being explored by Curiosity, including the Murray formation. The Cwd western dark unit is particularly well defined due to its low albedo in comparison with the surrounding units (Figure 14). The thickness of this unit is approximately 20 m at its southwestern extent, based on the height of the cliff as computed from a HiRISE DEM and assuming horizontal emplacement. Two smaller cliff-forming units, characterized by their smooth appearance and light and medium albedos (Csl and Csm, respectively), are found in the south of the mapping area and are characterized by appearing similarly competent and spectrally bland. The majority of these two units, however, are covered in sand dunes.

A hummocky terrain unit is identifiable between the eastern and western cliff-forming units. Within this terrain there are three subregions, discriminated by texture: smoother hummocky (Hs), rougher hummocky (Hr), and polygonally fractured hydroxylated Hummocky (Hph). The polygonally fractured unit (Hph) is characterized by a distinct, smaller-scale texture of polygonal fractures, each approximately a few meters wide

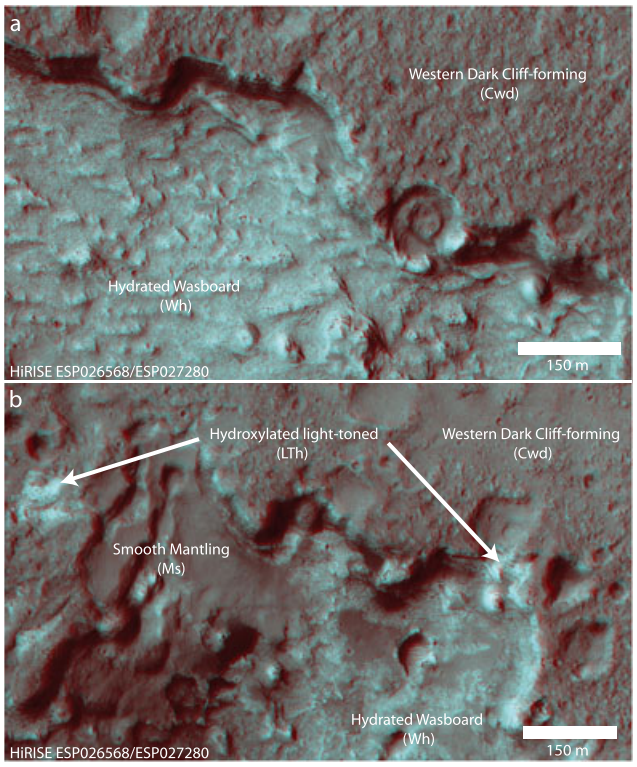

Figure 14. HiRISE (ESP 026568 and ESP 027280) anaglyphs of contacts at the western edge of a capping unit. (a) The phyllosilicate-bearing unit of preserved bed forms (Wh), characterized by distinct lithified linear dunes with a "washboard texture" as described by *Milliken et al*. [2014], has a sharp contact with the overlying spectrally bland and expansive cliff-forming unit (Cwd). (b) At higher elevations a hydroxylated light-toned unit (LTh) appears between the washboard unit and the cliff-forming unit. There also appears to be a later event, which deposited a dark, bland, mantling material (Ms) onto all three units. Our interpretive stratigraphic column is shown in Figure 20.

(Figure 15). The polygonal fracturing is coincident with spectral signatures of hydroxylation in CRISM data (scene 28B4, section 4.2.4). The rougher and smoother hummocky units are distinguished based on the size and the frequency of the hills found within them. The differences between the subregions of this hummocky terrain may represent lateral variations within the unit or postdepositional changes segregated to different elevations.

Two small light-toned units were mapped: the northern light toned (LTn) and the hydroxylated light toned (LTh), the latter exposed in Figure 14. In common between these units is their high albedo and thin, recessive, nature. The hydroxylated light-toned (LTh) unit is so named because the CRISM coverage over it indicates a distinctive signature of hydroxylated minerals discussed in section 4.2.4. Although nearby and at a similar elevation to the polygonally fractured hummocky unit, it is texturally distinct. CRISM coverage over the northern light-toned (LTn) unit does not reveal any distinguishable mineralogy, but this may be due to dust cover.

As previously mentioned the two hydroxylated units have similar wavelength absorptions in both the 1.4 and 2.3 μm regions indicating a similar mineralogy (Figure 4). The washboard (Wh) unit has metal-OH absorptions at similar wavelengths but also includes the 1.9 μm water absorption. Interestingly, these spectra have absorptions at similar wavelengths to the phyllosilicates detected in Farah Vallis and on the western Gale wall (CRISM scenes 2456A and 9D8A, respectively).

A mysterious dark depression approximately 3 km across (Figure 16) is almost completely surrounded by the hummocky terrain. Within the depression is a smooth material with a comparatively lower albedo, mapped as smooth depression (Ds). At the center of this smooth depression the material is highly polygonally fractured with raised ridges (Figure 16 inset). Additionally, large preserved linear ridges (Lrp) are present within the depression in close proximity to the fractures. These linear ridges are distinct from the polygonal ridges as they are in sets of parallel clusters (i.e., do not intersect). The stratigraphic relationship between this depression, the linear ridges, and the hummocky terrain is not clear from the data available, i.e., whether the ridges only exist within the depression or whether they are in an underlying unit that crops out only in the depression.

4.3.3. Exposed Stratigraphy

Many of the stratigraphic relationships are hard to determine from orbit due to limits in the image and topographic resolution or because the contacts are obscured by dust, sand, or other units. However, a combination of image data sets and topography has allowed us to determine some of the stratigraphic relationships.

HiRISE anaglyphs (Figures 14 and 15) and DEMs (Figure 13, top) over the western dark cliff-forming (Cwd) unit and adjacent exposures show a clear contact: the Cwd overlies a thin exposure of light-toned hydroxylated unit (LTh), which in turn overlies the washboard unit (Wh). The cliff-forming unit (Cwd) also overlies

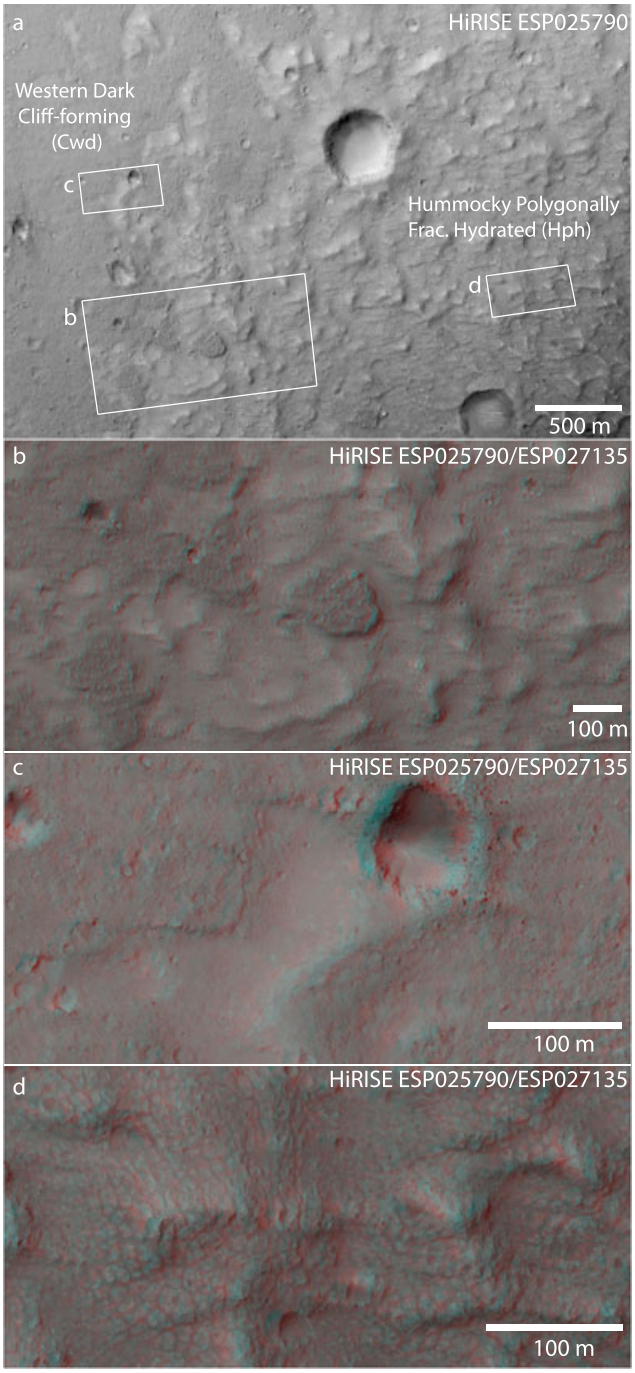

Figure 15. (a) CTX image showing the contact between the dark capping unit (Cwd) (west) and hummocky polygonally fractured unit (Hph) (east). (b) HiRISE anaglyph showing how Cwd appears to fill in topographic lows from Hph in an embaying relationship. (c) HiRISE anaglyph showing Hph emerging from below Cwd at a topographic high. (d) HiRISE anaglyph showing a type section of Hph with several meter-scale polygonal fractures.

the polygonally fractured hummocky unit (Hph) and fills in depressions within the hummocky terrain (Figure 15). Cwd, LTh, and Wh are all partially overlain by a small deposit of a dark mantling material (Ms) (Figure 14).

A profile taken near the base of Mount Sharp shows some of the elevation extents of the mapped units (Figure 13, top). Apparent in this profile is the flat surface created by the western cliff-forming (Cwd) unit and the hilly nature of the hummocky unit (Hr/Hs/Hph). Overall, the floor units are generally flat and gently dropping in elevation from the base of the Gale rim toward Mount Sharp (Figure 13, middle).

The contact of the Murray formation [from *Grotzinger et al*., 2015; *Fraeman et al*., 2016] with the units mapped in this study (eastern cliff-forming (Ced) and rough and polygonally fractured hummocky units (Hr and Hph, respectively)) does not occur at a single elevation. Rather, the Murray appears to have significant vertical and lateral extent, meeting each unit at a different elevation. Rover-scale observations just east of our study region show that the Bradbury group, which corresponds to some of our mapped units (for example, the eastern and pock-marked cliff-forming units (Ced and Cpm, respectively)), interfingers with and overlies the Murray unit [*Grotzinger et al*., 2015].

A unique window into the stratigraphy of the Gale floor sedimentary deposits is provided by a relatively fresh ~4 km crater, the walls of which expose multiple geologic units spanning >250 m of continuous section (Figure 17). While the crater from Figure 10 does not demonstrate any distinguishable layering, the crater from Figure 17 has multiple identifiable units. The uppermost portion of the crater wall is characterized by brecciated material with meter-sized blocks and occasional light-toned fracture fill. The topographic profile of the crater (Figure 17c) shows that the breccia is limited to the region above the existing landscape and, therefore, likely represents disrupted materials and the crater ejecta. Outside of the crater, the northern light-toned (LTn) unit is below the dark ejecta blanket and the dark pock-marked cliff-

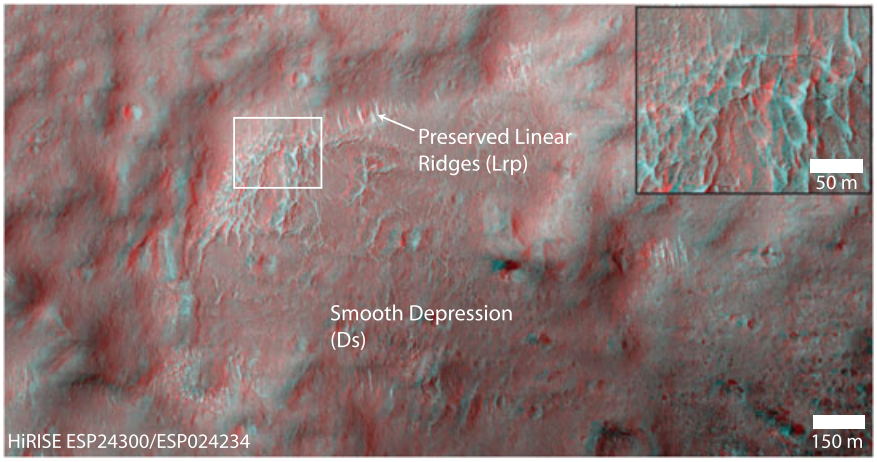

Figure 16. HiRISE anaglyph of the bottom of a smooth depression (Ds) on the Gale floor. Along the edges of the depression raised polygonal (inset) ridges and preserved linear ridges (Lrp) are present.

forming unit, Cpm. This light-toned unit does not seem to be exposed within the crater. Below the brecciated unit relatively competent material is exposed, expressed as the large knobs (Figure 17b). This knobby material overlies several recessive units, which form a well-bedded, ~90 m thick layered sequence with alternating light and dark gray tones (Figure 17b). This 4 km crater excavates the deepest sedimentary units exposed within Gale crater. Its base is ~50 m below the lowest elevation explored by Curiosity (just east of Yellowknife Bay). A comparison of the depth of materials exposed within this crater with those mapped elsewhere on the northwest Gale floor shows that the recessive layers lie below the other units (Figure 18). In fact, the topographic extent of all of the orbitally mapped units is above or within the elevation boundaries of the knob-forming layer. Thus, the ~90 m layered sequence of light-dark units represent the lowest elevation sedimentary units exposed in Gale crater. The layered sedimentary units extend to the base of the crater, indicating that Gale impact-related bedrock is not exposed. CRISM coverage is available in this crater, though no mineral detections were made.

5. Discussion

5.1. The Mineralogy of Gale Crater's Rim and Walls

Olivine and hydrated silicates are relatively widespread within the Gale crater rim and wall materials, extending previous scattered detections by *Wray* [2013] and *Ehlmann and Buz* [2015]. Around the western rim of Gale and in the portions to the southwest incised by Farah Vallis, the competent bedrock that comprises Gale crater's upper rim materials is olivine bearing. No feldspar-rich lithologies were observed in CRISM or THEMIS data, though obscuration by dust cover precludes a truly comprehensive survey. Very small outcrops with mineral detections present in targeted CRISM scenes indicate that a fruitful avenue for further investigation will be analyses of additional CRISM-targeted data acquired of the Gale rim. These future data remain the best near-term means available for identifying potentially feldspar-rich lithologies in the Gale rim that may be related to the more alkali-rich or felsic float rocks detected by Curiosity [*Stolper et al*., 2013; *Sautter et al*., 2014; *Thompson et al*., 2015].

Rim rock outcrops also contain Fe/Mg phyllosilicates, seen most clearly in the boulder-rich upper reaches of Farah Vallis. However, the timing of phyllosilicate formation is ambiguous: alteration of the rim bedrock may predate Gale crater formation or have occurred any time thereafter. Materials lower down on the walls of Gale crater—either mass-wasted bedrock materials or overlying sediments—also have signatures of olivine and Fe/Mg phyllosilicates, sometimes found within the same pixels (e.g., image 9D8A; Figures 4 and 9).

There is notable variability in band center wavelength and strength in the absorptions related to hydration and hydroxylation. Units with 1.9 μm absorptions characteristic of hydrated minerals are seen in the crater ejecta from 1791F and also in eastern Gale. Units without the 1.9 μm absorption but with Fe/Mg-OH

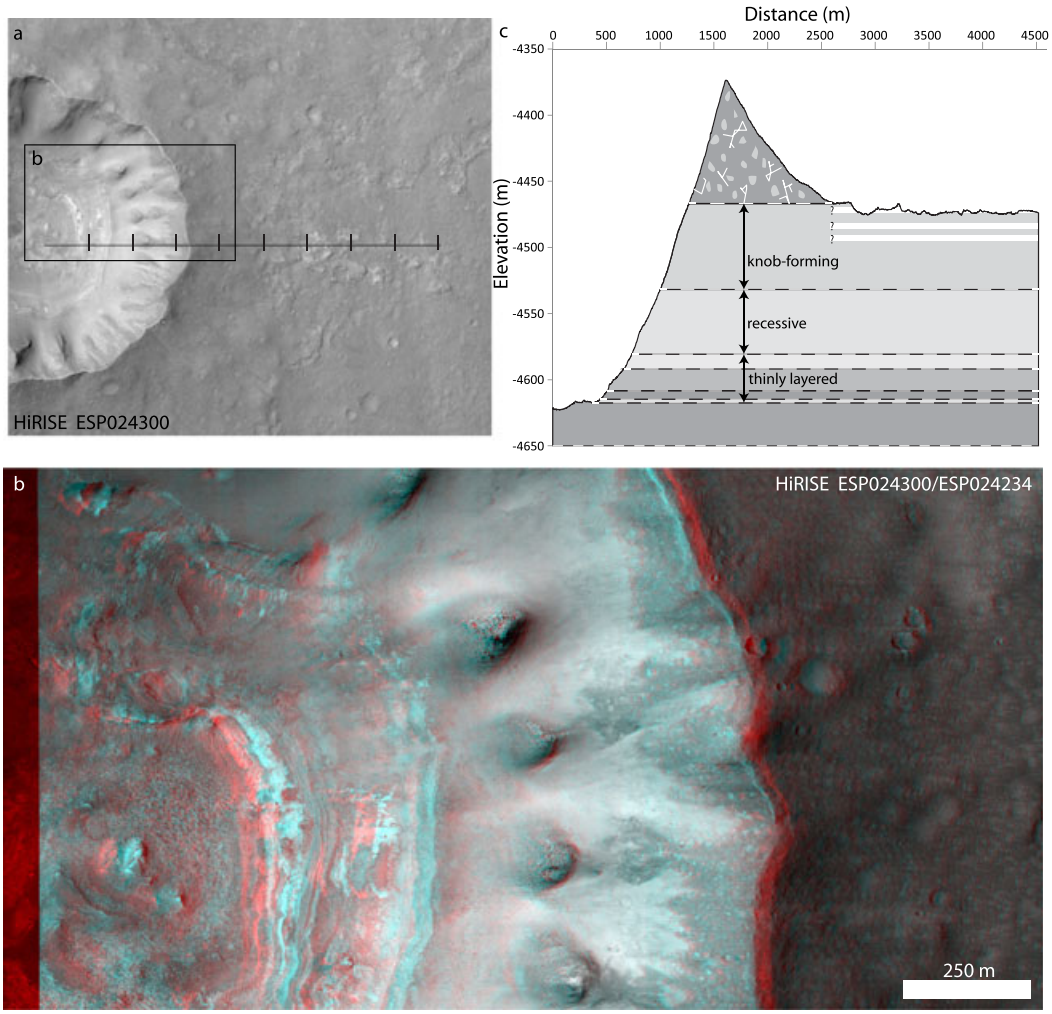

Figure 17. An ~4 km diameter fresh crater has impacted the northern Gale floor (see Figure 12 for context). (a) The underlying stratigraphy is clearly seen on the crater walls in HiRISE ESP024300. East of the crater ejecta lie shallowly exposed light-toned deposits, which are indicated in Figure 17c by horizontal white lines. (b) HiRISE anaglyph of fresh crater. The bottom of the crater is layered, indicating that despite the crater's depth, sedimentary units are sampled; and the materials exposed by the crater do not reach the Gale basement. (c) A HiRISE DEM permits estimating the bed thicknesses exposed within the crater, along the profile in Figure 17a, assuming roughly horizontal bedding. The units observed have been used in our inferred sequence of events in Figure 20.

absorptions are present on the Gale floor (in scenes 28B4 and 1791F). Detections with both hydration and hydroxylation are seen primarily on the Gale wall/rim. There is significant variability in the exact band position for both the 1.4 μm and 2.3 μm absorptions (Figure 19). When comparing the band positions of these absorptions with that of library spectra, we observe that overall, the absorptions mostly cluster near nontronite but that some spectra are more characteristic of Fe saponites (Figure 19). Thus, the orbital data imply dioctahedral and trioctahedral phyllosilicates, varying in composition by location. Some of the olivine-bearing materials are also hydrated/hydroxylated, which could indicate their alteration by interaction with water.

5.2. Potential Sulfates or Zeolites on the Eastern Gale Rim

A novel finding of this work is the detection of materials with 1.92 μm and 2.48 μm absorption features in the eastern Gale rim rocks. Both absorptions are consistent with their cause being water (H_2O) in the mineral structure. Current spectral data do not permit a unique identification of the phase. One candidate for these detections are zeolite minerals, including calcium and sodium zeolites which have water-related

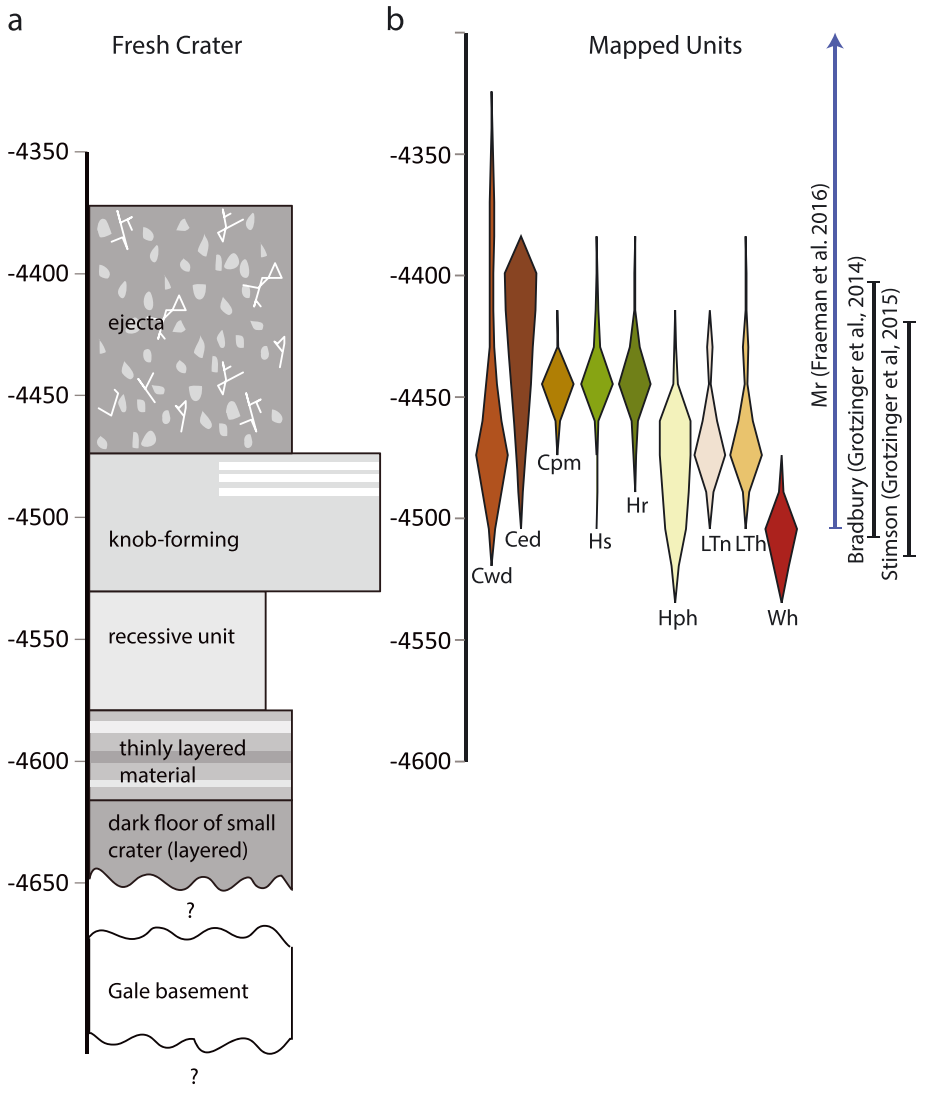

Figure 18. (a) Stratigraphic column of the fresh crater in Figure 17. Using a HiRISE DEM (DTEEC ESP 024234 and ESP 024300), we are able to estimate the thickness of the units exposed in the walls. A coarse breccia with fracture fill is seen in the uppermost layers of the crater; the elevation profile indicates that this breccia is likely ejecta and/or impact-disrupted materials. Light-toned material crops out to the east of the crater, though does not appear to extend into the crater. An especially competent unit erodes into knobs along the wall of the crater; below it is a bland recessive unit. The lowermost units in the crater are finely layered with alternating light and dark bands. (b) Elevation extents of a subset of the mapped units as well as the Murray unit as mapped in prior work [*Fraeman et al.*, 2016]. The elevation ranges observed in the mapped units further demonstrate that the stratigraphy is complex, likely with multiple unconformities, as many of the units have overlapping vertical extents.

absorptions in similar positions [*Cloutis et al.*, 2002]. Zeolite minerals have been previously found on Mars and represent low-temperature hydrothermal fluid circulation or diagenesis in highly alkaline systems with peak temperatures $<$ ~300°C [*Arkai et al.*, 2003; *Hay*, 2009; *Ehlmann et al.*, 2011]. A second possibility is sulfates. Spectra from the eastern rim are similar to, but not uniquely matched to, the hydrated calcium sulfate bassanite, which has also been detected by the Curiosity rover and which formed from diagenesis [*Vaniman et al.*, 2014]. When compared with the sulfates identified in *Fraeman et al.* [2016], the absorptions in the eastern rim rocks are similarly broad though appear at a shorter wavelength (Figure 5). Topography shows that the minerals on the eastern rim occur at an elevation that is ~2 km higher than those sulfates in the mound. Thus, these hydrated materials along the eastern Gale rim are intriguing but additional identified exposures will be required to determine their origin and relationship —if any—to sulfates in Mount Sharp.

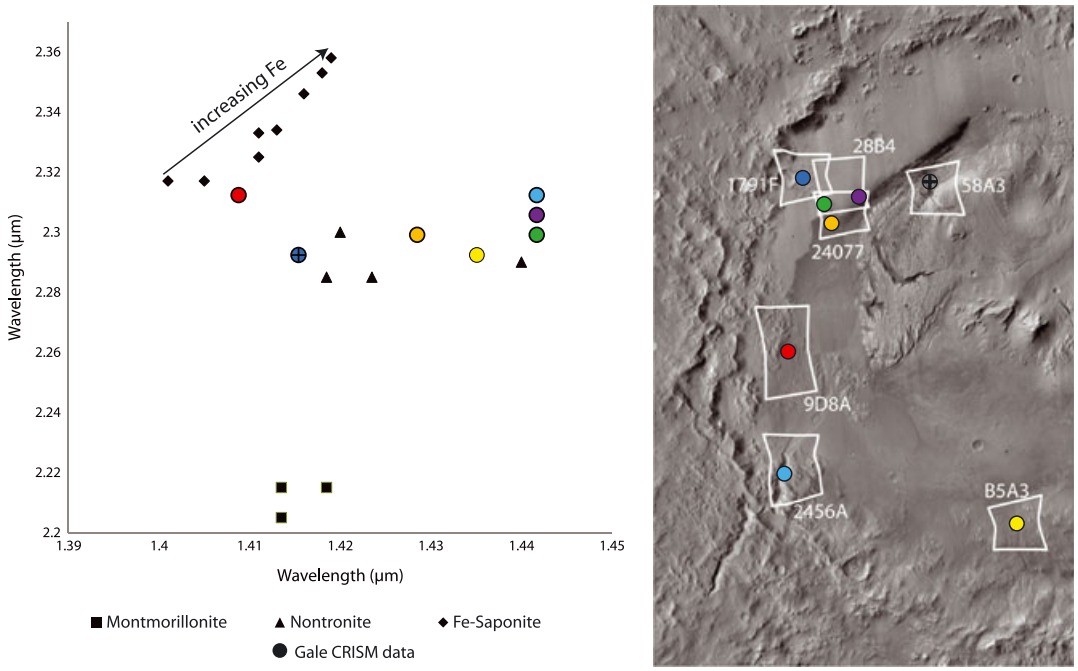

Figure 19. Plot of 1.4 and 2.3 μm band centers of our remote sensing observations and comparison with library spectra. Colored circles correspond to the CRISM images from Gale at the right, and band centers were computed from the spectra in Figure 4. Library spectra were taken from the U.S. Geological Survey spectral library [*Clark et al*., 2007], Reflectance Experiment Laboratory spectra used in *Michalski et al*. [2015] and *Cuadros et al*. [2013], as well as ferrous saponites measured in a Mars-like environment from *Chemtob et al*. [2015]. In the case of our detections, the shorter wavelength absorption is more diagnostic of mineral composition since it has a broader range. The comparison indicates that we are likely observing phyllosilicates near the nontronite end of the smectite continuum.

5.3. Gale Walls as Source for Floor Material

The rim and wall materials have certainly contributed to the floor sediments and sedimentary rocks by ongoing erosion of Gale crater's walls. Some morphological features are clearly related to mass wasting, such as the landslides seen in CRISM scenes B5A3 and 2456A (Figures 7 and 8, respectively). Others are fluvial, such as inverted channels on the NW Gale floor (Figure 12) and Peace Vallis. Consistent with this observation, previous mapping has indicated that some of the floor deposits originated from bedrock channels incised into the crater walls [e.g., *Le Deit et al*., 2013]. The majority of the hydrated mineral detections in the rim and wall are within areas with apparent fluvial, alluvial, or mass wasting activity. In particular, recent landslides in scenes 2456A and B5A3 contain phyllosilicates. *Watkins et al*. [2015] previously studied the association between clays and landslides in Valles Marineris, suggesting that clays may facilitate landsliding, a conclusion which may be relevant to Gale. Alternatively, phyllosilicates may not cause or facilitate sliding but simply be best exposed in these deposits because they are more recent and less dust covered.

Phyllosilicate mineral detections made on the wall and rim of Gale crater have absorptions in the 2.1 μm to 2.4 μm range, with the metal-OH band minima centered near 2.28–2.32 μm, suggesting Fe/Mg smectites, ranging from dioctahedral nontronite to trioctahedral saponite (Figures 4 and 19). Some rim/wall rocks are Fe-saponite bearing, similar compositionally to the clay minerals detected at Yellowknife Bay. One simple scenario is that the materials transported to the Gale floor were already partially altered from the original protolith and that the clay minerals are mostly detrital, derived from the rim rocks. In this scenario, further transformation and mineral precipitation might then take place as diagenesis proceeded during burial (similar to the process hypothesized by *Ehlmann and Buz* [2015] and *Schieber et al*. [2017]). However, the similarities between the mineral assemblages detected orbitally and those detected by the rover and on the Gale floor do not require a common origin. A potential alternative scenario is that bedrock at each locality started with a similar mafic-type composition and later underwent alteration due to local lacustrine or diagenetic aqueous activity (the original hypothesis for the Yellowknife Bay locality [*Vaniman et al*., 2014; *Bristow et al*., 2015]). In fact, textural studies of the Sheepbed mudstone at Yellowknife Bay indicate that the raised ridges [*Siebach et al*., 2014] and nodules [*Stack et al*., 2014] are of diagenetic origin. Furthermore, chemical

analyses of the raised ridges show a composition similar to an Fe or Mg smectite [*Léveillé et al*., 2014]. Both scenarios likely apply to rover-explored sedimentary rocks in different units; i.e., some clay minerals were transported from rim/wall units, and some were formed in situ. Some may have also then been altered by burial diagenesis. The hydroxylated units on the floor might represent clay-bearing sedimentary units of either origin that were dehydrated then exhumed. However, importantly, the rim/wall and floor unit spectral signatures indicate distinct chemistries from the Al nontronite detected from orbit in Mount Sharp's phyllosilicate unit [*Milliken et al*., 2010; *Fraeman et al*., 2016]. This suggests either different protoliths or different water chemistries to explain the distinct clay chemistry between the units in the walls and floor and those in units yet to be explored by the rover in Mount Sharp.

5.4. Potential Lacustrine Deposits and Evidence for Groundwater Diagenesis

Many units in our study area share characteristics with the lacustrine or distal fluvial units traversed by the Curiosity rover [*Grotzinger et al*., 2014, 2015]. The strongest evidence for lacustrine sedimentary rocks is in the alternating light and dark layers found within the fresh crater from Figure 17, which mimic small-scale bedding sequences seen in sediments from lacustrine environments on Earth [*Bohacs et al*., 2003]. At least 20 distinct thin layers are visible within an ~90 m sedimentary stack. The layered sediments in the fresh crater are also considerably more recessive in comparison with the knob-forming unit above them, which would be expected for less resistant materials such as siltstones or mudstones. Assuming roughly flat-lying units such that elevation is a proxy for age, these lake deposits likely predate those investigated at Yellowknife Bay by the rover. The thinly layered materials of the fresh crater may be stratigraphically older facies, equivalents of the Murray and Sheepbed mudstones. This interpretation could be consistent with a long-lived lake whose shore receded away from the crater rim with time [*Grotzinger et al*., 2015]. Alternatively, episodically present lakes where the depth fluctuated repeatedly might explain the thickness of the strata and the variation in properties in the layered sequence. The massive, comparatively more competent, knob-forming layer may represent a capping sandstone on these thinly layered deposits, in a similar manner to the capping units seen by the Curiosity rover [*Grotzinger et al*., 2014, 2015]. Without in situ data on these strata and their decameter- to millimeter-scale textures, it is not possible to definitively discriminate between these scenarios.

The mapped floor units in NW Gale crater show a transition from readily eroded recessive units to competent, cliff-forming units. A similar pattern is also observed in the relatively fresh 4 km diameter crater walls (Figure 17), which transition from thinly layered material to knob-forming materials. However, the materials exposed in the crater and floor units occur at different elevations. This may indicate that transitions of this style are episodic and have occurred multiple times. Lacustrine units potentially include the light-toned units (LTn and LTh) and the Hph polygonally fractured and hydroxylated hummocky unit. All three units are recessive, consistent with being composed of easily eroded fine-grained sedimentary rocks. They all underlie cliff-forming units similar to the knob-forming unit of the fresh crater. The hydroxylation in LTh and Hph is consistent with formation in or interaction with an aqueous environment. A final observation is the greater than or equal to meter-scale fracturing in the hummocky unit. If the sedimentary rocks are lacustrine, the fractures may have resulted from desiccation or freeze-thaw cycles. Alternative explanations for the fractures include unloading of previously buried material and weathering along fracture surfaces.

Regardless of the past extent of lakes on the Gale floor and their expression in these units, there is evidence for groundwater diagenesis. The polygonal ridges within the smooth depression (Ds) are consistent with mineralization along fractures by groundwater (Figure 16). Diagenetic alteration to form clay minerals within aeolian sandstones has been previously proposed to explain the spectral properties and corrugated appearance of the hydrated washboard unit [*Milliken et al*., 2014].

5.5. Stratigraphically Younger, Spectrally Bland, Cliff-Forming Materials

A distinguishing feature of the cliff-forming units, when compared with other mapped floor units, is their apparent spectral blandness, i.e., the lack of any electronic or vibrational absorptions to discriminate the units from a dusty or basaltic background suite of materials. Given the roughly homogeneous dust cover among all mapped units, there are at least three possible explanations for the unique lack of spectral features in the cliff-forming units: (1) Under a scenario of mass wasting or fluvial/aeolian transport from the crater rim, the hydrated silicates and mafics may have become diluted and be present in abundances below the detection limit. (2) The absence of hydrated/hydroxylated phases could also be consistent with

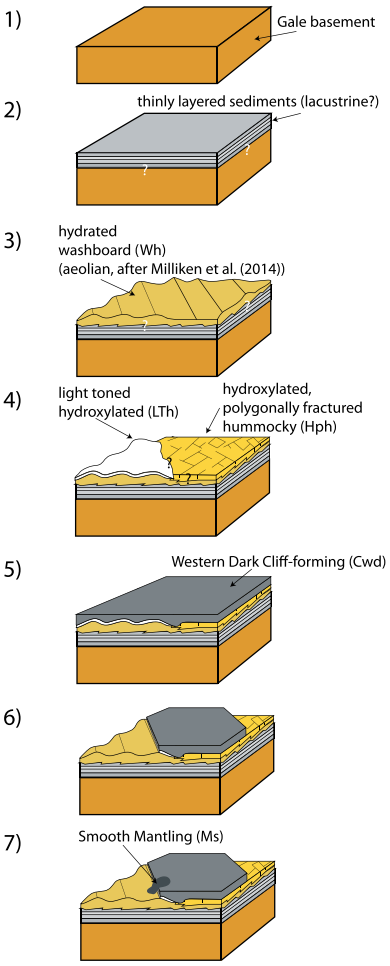

Figure 20. Schematic of the potential evolution of Gale crater floor sediments: (1) Gale crater is formed by a large impact, exposing basement rock (including potential impact melt sheets/impact-disrupted materials). (2) Sometime later, >100 m of thinly layered sediments which alternate in brightness are deposited in extensive units on the paleofloor of Gale (as seen in the fresh crater from Figure 17). These may be the result of a lacustrine environment. The exact contact relationship between these sediments and the Gale basement floor is unknown (indicated by a white question mark). (3) Perhaps due to a shallowing of the water present in Gale and the emplacement of sand dunes (as originally interpreted by *Milliken et al*. [2014] to explain the washboard morphology), the hydrated washboard (Wh) and hydroxylated polygonally fractured unit (Hph) are formed above the sediments. Although there is no clear contact between Wh, Hph, and the thinly laminated sediments, the stratigraphy seen in the fresh crater from Figure 17 indicates that the former two likely overly the latter. The uncertainty is again indicated by white question marks. (4) A localized zone of a light-toned hydroxylated material (LTh) is seen stratigraphically above Wh, formed, e.g., by evaporite deposition atop an aeolian unit as drawn here. The relationship between LTh and Hph, both of which are hydroxylated units, is obscured by a cap. The relationship between LTh and Wh may be related by sequential units in time: LTh as an alteration of the Wh or LTh as alteration at the base of the overlying spectrally bland cliff-forming unit. (5) A spectrally bland and extensive cliff-forming unit (Cwd) covers Wh, LTh, and Hph. This unit is competent and may represent a sandstone, fluvially facilitated mass wasting from the crater wall, or emplacement of an air fall deposit. (6) Erosion carves the cliff-forming unit back revealing the underlying sandstone and polygonally fractured unit. (7) A spectrally bland mantling unit (Ms) partially covers Cwd, LTh, and Wh.

declining lacustrine and groundwater activity through time and/or inhibition of mineralization during any water-assisted deposition under drier, colder conditions. (3) In an air fall source scenario, the material may be spectrally bland (dust rich or feldspar rich). The first two scenarios are not mutually exclusive. Without additional evidence for an air fall scenario, we interpret these cliff-forming units as sandstones, possibly similar to rover-observed Bradbury and Stimson caprock units [*Williams et al*., 2013; *Edgett et al*., 2016]. Additionally, our mapped boundaries for the Ced eastern dark cliff-forming unit and the Cpm pock-marked cliff-forming unit are partially coincident with previous mapping of a cratered surface and rough terrain of *Grotzinger et al*. [2014]. As with the rover-explored units, the observed diversity in cliff-forming morphology results from different dominant modes of deposition (aeolian versus fluvial versus mass wasting) or different styles of diagenesis.

5.6. Inferred Environmental History

We propose one potential formation scenario for the northern Gale floor, based on observations of the Gale rim rocks, floor sediments, and sedimentary rocks of the Murray formation explored by the Curiosity rover team (Figure 20). At the base of the sedimentary succession lies the Gale basement, an olivine-bearing suite of rocks impacted during Gale crater formation in the late Noachian/early Hesperian. Because the Gale basement is not exposed, it is unknown if anything lies between it and the lowest in elevation sedimentary unit observed, the thinly layered sedimentary rocks from the fresh crater in Figure 17. Regardless, sometime after crater formation, a ~90 m thick succession of finely stratified sediments was deposited on the Gale floor, which we hypothesize were likely lake deposits. Concurrently or shortly thereafter, a series of hydrated and hydroxylated units were emplaced. The Hph hummocky unit is

the most spatially extensive, containing dehydrated Fe/Mg phyllosilicates and showing a polygonally fractured morphology. The washboard unit (Wh) has hydrated Fe/Mg phyllosilicates associated with paleoaeolian deposits [*Milliken et al*., 2014] and occupies a similar elevation range to the Hph hummocky unit and similar stratigraphic position, beneath a cliff-forming unit (Figure 18). If the Hph hummocky and Wh washboard units are from a lacustrine or perilacustrine environment, one possible chronology may be a time-equivalent lateral transition from lake sediments to mud flats then to sand dunes. Small exposures of light-toned hydroxylated materials (LTh) are exposed stratigraphically above the washboard only; a contact relationship with the hummocky unit is not observed. The spectral similarities between the polygonally fractured hummocky unit (Hph) and the LTh hydroxylated light-toned deposits may indicate that the two units are closely related or perhaps that LTh is the thin distal portion of the hummocky unit (though does not share the same polygonal fracturing).

The transition from the hydrated washboard to the hydroxylated light-toned unit and then to the spectrally bland Cwd cliff-forming unit could have resulted from a variety of scenarios. Three plausible explanations for this sequence are (1) the LTh light-toned unit is the alteration product of the washboard unit, (2) the LTh light-toned unit is a separate unit from the Wh washboard and Cwd cliff-forming units, or (3) the LTh light-toned unit is the alteration product of the Cwd cliff-forming unit. One environmental scenario that may explain the sequence is a series of shallow lakes with relatively drier intervals (forming aeolian units) and wetter intervals (leaving light-toned polygonally fractured fine-grained sedimentary deposits upon evaporation). Aeolian units may have been cemented by minerals precipitated during groundwater upwelling. Lacustrine units explored by the Curiosity rover show abundant evidence for multiple episodes of diagenetic alteration [*Grotzinger et al*., 2014; *Nachon et al*., 2014; *Kah*, 2015; *Kronyak et al*., 2015]. Following the major water-related events, the spectrally bland cliff-forming units were emplaced and then later eroded leaving the landscapes seen today. Some more recent mantling and crater ejecta material has been emplaced in discrete locations superposing sequences of stratigraphic units (such as in Figure 14b).

All data from orbit are consistent with the scenario outlined above; nevertheless, confirmation of this would require viewing the context and textures at submeter or subcentimeter resolution. Evidence for environmental scenarios that we propose might be found in the units that lie ahead in the Curiosity rover traverse.

6. Conclusions

The following are the key findings from our joint analysis of the Gale crater rim, wall, and floor units, which used CRISM and THEMIS spectroscopic data and high-resolution imagery, coupled with geologic mapping:

1. Extensive olivine- and Fe/Mg phyllosilicate-bearing materials were identified in the Gale wall, rim, and floor. No distinctly felsic materials were found, though detection capabilities are diminished by image artifacts and dust cover.
2. The Mount Sharp Fe/Al phyllosilicates are spectrally distinct from the Fe/Mg phyllosilicates observed on the wall, rim, and floor of Gale crater from orbit
3. Some of the floor phyllosilicates, including those observed at Yellowknife Bay by MSL, may be in part detrital with already altered sediments (olivine altered to Fe/Mg smectite) having been transported to the Gale floor. Alternative scenarios involve widespread alteration of rim and wall rocks and floor sediments by waters of similar chemistry.
4. Sedimentary deposits within Gale crater near the rover landing site are $>$250 m thick and include an ~90 m thick succession of thinly layered sedimentary rocks, possibly formed in an ancient lake(s). Relative to the units observed with Curiosity [*Grotzinger et al*., 2014, 2015], these findings extend the stratigraphic record of lake(s) within Gale crater.
5. Stratigraphic relationships between floor units with different characteristics may indicate alternating aeolian and lacustrine environments with different amounts of surface or groundwater. Contemporaneous lateral variations as well as possible multiple arid/wet cycles may have produced the observed sequences.
6. Cliff-forming units on top of the floor strata have no evidence for hydrated minerals, may postdate the most water-rich periods, and may be similar to the sandstones observed with the Curiosity rover.
7. Dramatic representations of recent and/or ongoing erosion, including landsliding, are observed on the Gale rim and walls.

The source of the feldspar-rich lithologies observed by the Curiosity rover still remains a mystery. Targeted CRISM data over more of the Gale rim and wall will be the best source of new data to continue the search for Fe-bearing feldspars and additional minerals. Additional spectral analysis, including use of oversampled data and new noise reduction techniques, may help elucidate the relationship between the floor and wall/rim lithologies. Supplementary HiRISE imagery will allow for more stratigraphic relationships to be determined and may allow further characterization of the units identified on the floor.

Acknowledgments
All data used in this paper are available in the NASA Planetary Data System; derived products are available by request. Thanks to efforts of the many spacecraft and instrument teams for their collection of these right data sets. Thanks to Ara Oshagan, Christopher Edwards, and Daven Quinn for assistance with data processing. J.B. was supported by a NASA Earth and Space Sciences Fellowship NNX15AQ95H for the conduct of this work. Partial support was also provided by an MSL Participating Scientist grant to B.L.E. We also thank Sanjeev Gupta and an anonymous reviewer for their comments and suggestions, which have improved this manuscript.

References

Anderson, R., and J. Bell (2010), Geologic mapping and characterization of Gale Crater and implications for its potential as a Mars Science Laboratory landing site, *Mars*, *5*, 76–128, doi:10.1555/mars.2010.0004.

Arkai, P., F. Sassi, and J. Desmons (2003), A systematic nomenclature for metamorphic rocks: 5. Very low-to low-grade metamorphic rocks, *Recommendations by the IUGS Subcommission on the systematics of metamorphic rocks*.

Bandfield, J., D. Rogers, M. Smith, and P. Christensen (2004), Atmospheric correction and surface spectral unit mapping using Thermal Emission Imaging System data, *J. Geophys. Res.*, *109*, E10008, doi:10.1029/2004JE002289.

Bandfield, J. L. (2009), Effects of surface roughness and graybody emissivity on Martian thermal infrared spectra, *Icarus*, *202*, 414–428, doi:10.1016/j.icarus.2009.03.031.

Bandfield, J. L., E. S. Amador, and N. H. Thomas (2013), Extensive hydrated silica materials in western Hellas Basin, Mars, *Icarus*, *226*, 1489–1498, doi:10.1016/j.icarus.2013.08.005.

Bandfield, J. L., V. E. Hamilton, and P. R. Christensen (2000), A global view of Martian surface compositions from MGS-TES, *Science*, *287*, 1626–1630, doi:10.1126/science.287.5458.1626.

Banham, S. G., S. Gupta, D. M. Rubin, J. A. Watkins, D. Sumner, J. Grotzinger, K. W. Lewis, K. S. Edgett, L. A. Edgar, and K. M. Stack (2016), Reconstruction of an ancient eolian dune field at Gale Crater, Mars: Sedimentary analysis of the Stimson formation, paper presented at LPSC, 2346, LPI Contributions, The Woodlands, Tex.

Bish, D. L., D. Blake, D. Vaniman, S. Chipera, R. Morris, D. Ming, A. Treiman, P. Sarrazin, S. Morrison, and R. Downs (2013), X-ray diffraction results from Mars Science Laboratory: Mineralogy of Rocknest at Gale Crater, *Science*, *341*(6153), 1,238,932–1,238,932, doi:10.1126/science.1238932.

Bishop, J., J. Madejova, P. Komadel, and H. Froschil (2002), The influence of structural Fe, Al, and Mg on the infrared OH bands in spectra of dioctahedral smectites, *Clay Miner.*, *37*, 607–616, doi:10.1180/0009855023740063.

Bishop, J. L., E. Z. N. Dobrea, N. K. McKeown, M. Parente, B. L. Ehlmann, J. R. Michalski, R. E. Milliken, F. Poulet, G. A. Swayze, and J. F. Mustard (2008), Phyllosilicate diversity and past aqueous activity revealed at Mawrth Vallis, Mars, *Science*, *321*, 830–833, doi:10.1126/science.1159699.

Bishop, J. L., E. Murad, and M. D. Dyar (2015), Akaganéite and schwertmannite: Spectral properties and geochemical implications of their possible presence on Mars, *Am. Mineral.*, *100*, 738–746, doi:10.2138/am-2015-5016.

Blake, D. F., R. Morris, G. Kocurek, S. Morrison, R. Downs, D. Bish, D. Ming, K. Edgett, D. Rubin, and W. Goetz (2013), Curiosity at Gale Crater, Mars: Characterization and analysis of the Rocknest sand shadow, *Science*, *341*(6153), 1239505, doi:10.1126/science.1239505.

Bohacs, K. M., A. R. Carrol, and J. E. Neal (2003), Lessons from large lake systems—Thresholds, nonlinearity, and strange attractors, *Geol. Soc. Am. Spec. Paper*, *370*, 75–90.

Bristow, T., et al. (2015), The origin and implications of clay minerals from Yellowknife Bay, Gale crater, Mars, *Am. Mineral.*, *100*, 824–836, doi:10.2138/am-2015-5077CCBYNCND.

Cabrol, N. A., E. A. Grin, H. E. Newsom, R. Landheim, and C. P. McKay (1999), Hydrogeologic evolution of Gale Crater and its relevance to the exobiological exploration of Mars, *Icarus*, *139*, 235–245, doi:10.1006/icar.1999.6099.

Carter, J., C. Viviano-Beck, D. Loizeau, J. Bishop, and L. Le Deit (2015), Orbital detection and implications of akaganéite on Mars, *Icarus*, *253*, 296–310, doi:10.1016/j.icarus.2015.01.020.

Chemtob, S. M., R. D. Nickerson, R. V. Morris, D. G. Agresti, and J. G. Catalano (2015), Synthesis and structural characterization of ferrous trioctahedral smectites: Implications for clay mineral genesis and detectability on Mars, *J. Geophys. Res. Planets*, *120*, 1119–1140, doi:10.1002/2014JE004763.

Christensen, P. R., B. M. Jakosky, H. H. Kieffer, M. C. Malin, H. Y. McSween Jr., K. Nealson, G. L. Mehall, S. H. Silverman, S. Ferry, and M. Caplinger (2004), The Thermal Emission Imaging System (THEMIS) for the Mars 2001 Odyssey mission, *Space Sci. Rev.*, *110*, 85–130, doi:10.1023/B:SPAC.0000021008.16305.94.

Christensen, P. R., et al. (2005), Evidence for magmatic evolution and diversity on Mars from infrared observations, *Nature*, *436*, 504–509, doi:10.1038/nature03639.

Clark, R. N., T. V. V. King, M. Klejwa, G. A. Swayze, and N. Vergo (1990), High spectral resolution reflectance spectroscopy of minerals, *J. Geophys. Res.*, *95*, 12653–12680, doi:10.1029/JB095iB08p12653.

Clark, R. N., G. A. Swayze, R. Wise, E. Livo, T. Hoefen, R. Kokaly, and S. J. Sutley (2007), USGS digital spectral library splib06a, *U.S. Geol. Surv., Digital Data Ser. 231*.

Cloutis, E. A., P. M. Asher, and S. A. Mertzman (2002), Spectral reflectance properties of zeolites and remote sensing implications, *J. Geophys. Res.*, *107*(E9), 5067, doi:10.1029/2000JE001467.

Cuadros, J., J. R. Michalski, V. Dekov, J. Bishop, S. Fiore, and M. D. Dyar (2013), Crystal-chemistry of interstratified Mg/Fe-clay minerals from seafloor hydrothermal sites, *Chem. Geol.*, *360–361*, 142–158, doi:10.1016/j.chemgeo.2013.10.016.

Edgett, K. S., et al. (2016), Recent observations by Curiosity's Mars Hand Lens Imager (MAHLI) of rock strata and eolian sediment on the lower north slope of Aeolis Mons, Gale Crater, Mars, paper presented at LPSC, 1382, LPI Contributions, The Woodlands, Tex., 1 March.

Ehlmann, B. L., and J. Buz (2015), Mineralogy and fluvial history of the watersheds of Gale, Knobel, and Sharp craters: A regional context for MSL Curiosity's exploration, *Geophys. Res. Lett.*, *42*, 264–273, doi:10.1002/2014GL062553.

Ehlmann, B. L., J. F. Mustard, R. N. Clark, G. A. Swayze, and S. L. Murchie (2011), Evidence for low-grade metamorphism, hydrothermal alteration, and diagenesis on Mars from phyllosilicate mineral assemblages, *Clays Clay Miner.*, *59*, 359–377, doi:10.1346/ccmn.2011.0590402.

Ehlmann, B. L., J. F. Mustard, G. A. Swayze, R. N. Clark, J. L. Bishop, F. Poulet, D. J. Des Marais, L. H. Roach, R. E. Milliken, and J. J. Wray (2009), Identification of hydrated silicate minerals on Mars using MRO-CRISM: Geologic context near Nili Fossae and implications for aqueous alteration, *J. Geophys. Res.*, *114*, E00D08, doi:10.1029/2009JE003339.

Fassett, C. I., and J. W. I. Head (2008), The timing of Martian valley network activity: Constraints from buffered crater counting, *Icarus*, *195*, 61–89, doi:10.1016/j.icarus.2007.12.009.

Fraeman, A., R. Arvidson, J. Catalano, J. Grotzinger, R. Morris, S. Murchie, K. Stack, D. Humm, J. McGovern, and F. Seelos (2013), A hematite-bearing layer in Gale Crater, Mars: Mapping and implications for past aqueous conditions, *Geology*, *41*, 1103–1106, doi:10.1130/G34613.1.

Fraeman, A. A., B. L. Ehlmann, R. E. Arvidson, C. S. Edwards, J. P. Grotzinger, R. E. Milliken, D. P. Quinn, and M. S. Rice (2016), The stratigraphy and evolution of lower Mt. Sharp from spectral, morphological, and thermophysical orbital datasets, *J. Geophys. Res. Planets*, *121*, 1713–1736, doi:10.1002/2016JE005095.

Grant, J. A., S. A. Wilson, N. Mangold, F. Calef, and J. P. Grotzinger (2014), The timing of alluvial activity in Gale Crater, Mars, *Geophys. Res. Lett.*, *41*, 1142–1149, doi:10.1002/2013GL058909.

Grotzinger, J. P., J. Crisp, A. R. Vasavada, R. C. Anderson, C. J. Baker, R. Barry, D. F. Blake, P. Conrad, K. S. Edgett, and B. Ferdowski (2012), Mars Science Laboratory mission and science investigation, *Space Sci. Rev.*, *170*, 5–56, doi:10.1007/s11214-012-9892-2.

Grotzinger, J. P., et al. (2014), A habitable fluvio-lacustrine environment at Yellowknife Bay, Gale Crater, Mars, *Science*, *343*(6169), 1242777, doi:10.1126/science.1242777.

Grotzinger, J. P., et al. (2015), Deposition, exhumation, and paleoclimate of an ancient lake deposit, Gale Crater, Mars, *Science*, *350*(6257), aac7575, doi:10.1126/science.aac7575.

Hay, R. (2009), Geologic occurrence of zeolites and some associated minerals, *Pure Appl. Chem.*, *58*, 1339–1342, doi:10.1351/pac198658101339.

Irwin, R. P., A. D. Howard, R. A. Craddock, and J. M. Moore (2005), An intense terminal epoch of widespread fluvial activity on early Mars: 2. Increased runoff and paleolake development, *J. Geophys. Res.*, *110*, E12S15, doi:10.1029/2005JE002460.

Kah, L. C. (2015), Late diagenetic cements in the Murray Formation, Gale Crater, Mars: Implications for postdepositional fluid flow, Abstract P53F-05 presented at 2015 Fall Meeting, AGU, San Francisco, Calif.

Kite, E. S., I. Halevy, M. A. Kahre, M. J. Wolff, and M. Manga (2013a), Seasonal melting and the formation of sedimentary rocks on Mars, with predictions for the Gale Crater mound, *Icarus*, *223*, 181–210, doi:10.1016/j.icarus.2012.11.034.

Kite, E. S., K. W. Lewis, M. P. Lamb, C. E. Newman, and M. I. Richardson (2013b), Growth and form of the mound in Gale Crater, Mars: Slope wind enhanced erosion and transport, *Geology*, *41*, 543–546, doi:10.1130/G33909.1.

Kreisch, C., R. Arvidson, J. O'Sullivan, K. Li, D. Politte, J. Finkel, E. Guinness, N. Stein, and A. Fraeman (2015), Log-likelihood method of reducing noise in CRISM along-track oversampled hyperspectral images, paper presented at Computational Optical Sensing and Imaging, Arlington, Va.

Kronyak, R. E., L. C. Kah, D. Blaney, D. Sumner, M. Fisk, W. Rapin, M. Nachon, N. Mangold, J. Grotzinger, and R. C. Wiens (2015), Garden City vein complex, Gale Crater, Mars: Implications for late diagenetic fluid flow, Abstract P43B-2122 presented at 2015 Fall Meeting, AGU, San Fransisco, Calif.

Lane, M. D., and P. R. Christensen (2013), Determining olivine composition of basaltic dunes in Gale Crater, Mars, from orbit: Awaiting ground truth from Curiosity, *Geophys. Res. Lett.*, *40*, 3517–3521, doi:10.1002/grl.50621.

Lapotre, M. G. A., B. L. Ehlmann, S. E. Minson, R. E. Arvidson, F. Ayoub, A. A. Fraeman, R. C. Ewing, and N. T. Bridges (2017), Compositional Variations in Sands of the Bagnold Dunes, Gale Crater, Mars, from Visible-Shortwave Infrared Spectroscopy and Comparison with Ground Truth from the Curiosity Rover, *J. Geophys. Res. Planets*, *122*, doi:10.1002/2016JE005133.

Le Deit, L., E. Hauber, F. Fueten, M. Pondrelli, A. P. Rossi, and R. Jaumann (2013), Sequence of infilling events in Gale Crater, Mars: Results from morphology, stratigraphy, and mineralogy, *J. Geophys. Res. Planets*, *118*, 2439–2473, doi:10.1002/2012JE004322.

Léveillé, R. J., et al. (2014), Chemistry of fracture-filling raised ridges in Yellowknife Bay, Gale Crater: Window into past aqueous activity and habitability on Mars, *J. Geophys. Res. Planets*, *119*, 2398–2415, doi:10.1002/2014JE004620.

Malin, M. C., and K. S. Edgett (2000), Sedimentary rocks of early Mars, *Science*, *290*, 1927–1937, doi:10.1126/science.290.5498.1927.

Malin, M. C., et al. (2007), Context Camera investigation on board the Mars Reconnaissance Orbiter, *J. Geophys. Res.*, *112*, E05S04, doi:10.1029/2006JE002808.

McEwen, A. S., et al. (2007), Mars Reconnaissance Orbiter's High Resolution Imaging Science Experiment (HiRISE), *J. Geophys. Res.*, *112*, E05S02, doi:10.1029/2005JE002605.

McLennan, S. M., et al. (2014), Elemental geochemistry of sedimentary rocks at Yellowknife Bay, Gale Crater, Mars, *Science*, *343*(6169), 1244734, doi:10.1126/science.1244734.

Michalski, J. R., J. Cuadros, J. L. Bishop, M. Darby Dyar, V. Dekov, and S. Fiore (2015), Constraints on the crystal-chemistry of Fe/Mg-rich smectitic clays on Mars and links to global alteration trends, *Earth Planet. Sci. Lett.*, *427*, 215–225, doi:10.1016/j.epsl.2015.06.020.

Milliken, R., J. Grotzinger, and B. Thomson (2010), Paleoclimate of Mars as captured by the stratigraphic record in Gale Crater, *Geophys. Res. Lett.*, *37*, L04201, doi:10.1029/2009GL041870.

Milliken, R. E., R. C. Ewing, W. W. Fischer, and J. Hurowitz (2014), Wind-blown sandstones cemented by sulfate and clay minerals in Gale Crater, Mars, *Geophys. Res. Lett.*, *41*, 1149–1154, doi:10.1002/2013GL059097.

Morgan, F., F. Seelos, S. Murchie, and C. Team (2009), CAT tutorial, paper presented at CRISM Data User's Workshop, Houston, Tex.

Murchie, S., et al. (2007), Compact Reconnaissance Imaging Spectrometer for Mars (CRISM) on Mars Reconnaissance Orbiter (MRO), *J. Geophys. Res.*, *112*, E05S03, doi:10.1029/2006JE002682.

Murchie, S. L., F. P. Seelos, C. D. Hash, D. C. Humm, E. Malaret, J. A. McGovern, T. H. Choo, K. D. Seelos, D. L. Buczkowski, and M. F. Morgan (2009), Compact Reconnaissance Imaging Spectrometer for Mars investigation and data set from the Mars Reconnaissance Orbiter's primary science phase, *J. Geophys. Res.*, *114*, E00D07, doi:10.1029/2009JE003344.

Nachon, M., et al. (2014), Calcium sulfate veins characterized by ChemCam/Curiosity at Gale crater, Mars, *J. Geophys. Res. Planets*, *119*, 1991–2016, doi:10.1002/2013JE004588.

Osterloo, M. M., F. S. Anderson, V. E. Hamilton, and B. M. Hynek (2010), Geologic context of proposed chloride-bearing materials on Mars, *J. Geophys. Res.*, *115*, E10012, doi:10.1029/2010JE003613.

Palucis, M. C., W. E. Dietrich, R. M. E. Williams, A. G. Hayes, T. Parker, D. Y. Sumner, N. Mangold, K. Lewis, and H. Newsom (2016), Sequence and relative timing of large lakes in Gale crater (Mars) after the formation of Mount Sharp, *J. Geophys. Res. Planets*, *121*, 472–496, doi:10.1002/2015JE004905.

Pan, L., B. L. Ehlmann, J. Carter, and C. M. Ernst (2015), Probing Mars' northern plains stratigraphy with impact craters, paper presented at LPSC, 2583, LPI Contributions, The Woodlands, Tex.

Pelkey, S., J. Mustard, S. Murchie, R. Clancy, M. Wolff, M. Smith, R. Milliken, J. P. Bibring, A. Gendrin, and F. Poulet (2007), CRISM multispectral summary products: Parameterizing mineral diversity on Mars from reflectance, *J. Geophys. Res.*, *112*, E08S14, doi:10.1029/2006JE002831.

Pelkey, S. M., and B. M. Jakosky (2002), Surficial geologic surveys of Gale Crater and Melas Chasma, Mars: Integration of remote-sensing data, *Icarus*, *160*, 228–257, doi:10.1006/icar.2002.6978.

Pelkey, S. M., B. M. Jakosky, and P. R. Christensen (2004), Surficial properties in Gale Crater, Mars, from Mars Odyssey THEMIS data, *Icarus*, *167*, 244–270, doi:10.1016/j.icarus.2003.09.013.

Poulet, F., J. Carter, J. L. Bishop, D. Loizeau, and S. M. Murchie (2014), Mineral abundances at the final four curiosity study sites and implications for their formation, *Icarus*, *231*, 65–76, doi:10.1016/j.icarus.2013.11.023.

Rogers, A. D., and J. L. Bandfield (2009), Mineralogical characterization of Mars Science Laboratory candidate landing sites from THEMIS and TES data, *Icarus*, *203*, 437–453, doi:10.1016/j.icarus.2009.04.020.

Rogers, A. D., and P. R. Christensen (2007), Surface mineralogy of Martian low-albedo regions from MGS-TES data: Implications for upper crustal evolution and surface alteration, *J. Geophys. Res.*, *112*, E01003, doi:10.1029/2006JE002727.

Rogers, A. D., and R. L. Fergason (2011), Regional-scale stratigraphy of surface units in Tyrrhena and Iapygia Terrae, Mars: Insights into highland crustal evolution and alteration history, *J. Geophys. Res.*, *116*, E08005, doi:10.1029/2010JE003772.

Rogers, A. D., P. R. Christensen, and J. L. Bandfield (2005), Compositional heterogeneity of the ancient Martian crust: Analysis of Ares Vallis bedrock with THEMIS and TES data, *J. Geophys. Res.*, *110*, E05010, doi:10.1029/2005JE002399.

Sautter, V., C. Fabre, O. Forni, M. Toplis, A. Cousin, A. Ollila, P. Meslin, S. Maurice, R. Wiens, and D. Baratoux (2014), Igneous mineralogy at Bradbury Rise: The first ChemCam campaign at Gale crater, *J. Geophys. Res. Planets*, *119*, 30–46, doi:10.1002/2013JE004472.

Schieber, J., D. Bish, M. Coleman, M. Reed, E. M. Hausrath, J. Cosgrove, S. Gupta, M. E. Minitti, K. S. Edgett, and M. Malin (2017), Encounters with an unearthly mudstone: Understanding the first mudstone found on Mars, *Sedimentology*, *64*, 311–358, doi:10.1111/sed.12318.

Schmidt, M. E., et al. (2014), Geochemical diversity in first rocks examined by the Curiosity Rover in Gale Crater: Evidence for and significance of an alkali and volatile-rich igneous source, *J. Geophys. Res. Planets*, *119*, 64–81, doi:10.1002/2013JE004481.

Seelos, K. D., F. P. Seelos, C. E. Viviano-Beck, S. L. Murchie, R. E. Arvidson, B. L. Ehlmann, and A. A. Fraeman (2014), Mineralogy of the MSL Curiosity landing site in Gale crater as observed by MRO/CRISM, *Geophys. Res. Lett.*, *41*, 4880–4887, doi:10.1002/2014GL060310.

Siebach, K. L., and J. P. Grotzinger (2014), Volumetric estimates of ancient water on Mount Sharp based on boxwork deposits, Gale Crater, Mars, *J. Geophys. Res. Planets*, *119*, 189–198, doi:10.1002/2013JE004508.

Siebach, K. L., M. B. Baker, J. P. Grotzinger, S. M. McLennan, R. Gellert, L. M. Thompson, and J. A. Hurowitz (2017), Sorting out compositional trends in sedimentary rocks of the Bradbury group (Aeolus Palus), Gale crater, Mars, *J. Geophys. Res. Planets*, *122*, 295–328, doi:10.1002/2016JE005195.

Siebach, K. L., J. P. Grotzinger, L. C. Kah, K. M. Stack, M. Malin, R. Léveillé, and D. Y. Sumner (2014), Subaqueous shrinkage cracks in the Sheepbed mudstone: Implications for early fluid diagenesis, Gale Crater, Mars, *J. Geophys. Res. Planets*, *119*, 1597–1613, doi:10.1002/2014JE004623.

Stack, K. M., et al. (2014), Diagenetic origin of nodules in the Sheepbed member, Yellowknife Bay formation, Gale crater, Mars, *J. Geophys. Res. Planets*, *119*, 1637–1664, doi:10.1002/2014JE004617.

Stolper, E. M., et al. (2013), The petrochemistry of Jake_M: A Martian mugearite, *Science*, *341*(6153), 1239463, doi:10.1126/science.1239463.

Sunshine, J. M., and C. M. Pieters (1998), Determining the composition of olivine from reflectance spectroscopy, *J. Geophys. Res.*, *103*, 13675–13688, doi:10.1029/98JE01217.

Szabo, T., G. Domokos, J. P. Grotzinger, and D. J. Jerolmack (2015), Reconstructing the transport history of pebbles on Mars, *Nat. Commun.*, *6*, 8366, doi:10.1038/ncomms9366.

Taylor, G. J., W. V. Boynton, S. M. McLennan, and L. M. V. Martel (2010), K and Cl concentrations on the Martian surface determined by the Mars Odyssey Gamma Ray Spectrometer: Implications for bulk halogen abundances in Mars, *Geophys. Res. Lett.*, *37*, *L12204*, doi:10.1029/2010GL043528.

Thompson, L., R. Gellert, J. G. Spray, L. C. Kah, and M. S. Team (2015), The composition of the basal Murray formation at Pahrump Hills, Gale Crater, Mars paper presented at LPSC, 1429, LPI Contributions, The Woodlands, Tex.

Thomson, B., N. Bridges, R. Milliken, A. Baldridge, S. Hook, J. Crowley, G. Marion, C. de Souza Filho, A. Brown, and C. Weitz (2011), Constraints on the origin and evolution of the layered mound in Gale Crater, Mars using Mars Reconnaissance Orbiter data, *Icarus*, *214*, 413–432, doi:10.1016/j.icarus.2011.05.002.

Treiman, A. H., et al. (2016), Mineralogy, provenance, and diagenesis of a potassic basaltic sandstone on Mars: CheMin X-ray diffraction of the Windjana sample (Kimberley area, Gale Crater), *J. Geophys. Res. Planets*, *121*, 75–106, doi:10.1002/2015JE004932.

Vaniman, D., D. Bish, D. Ming, T. Bristow, R. Morris, D. Blake, S. Chipera, S. Morrison, A. Treiman, and E. Rampe (2014), Mineralogy of a mudstone at Yellowknife Bay, Gale Crater, Mars, *Science*, *343*(6169), 1243480, doi:10.1126/science.1243480.

Viviano-Beck, C. E., et al. (2014), Revised CRISM spectral parameters and summary products based on the currently detected mineral diversity on Mars, *J. Geophys. Res. Planets*, *119*, 1403–1431, doi:10.1002/2014JE004627.

Watkins, J. A., B. L. Ehlmann, and A. Yin (2015), Long-runout landslides and the long-lasting effects of early water activity on Mars, *Geology*, *43*, 107–110, doi:10.1130/g36215.1.

Williams, R. M. E., et al. (2013), Martian fluvial conglomerates at Gale Crater, *Science*, *340*, 1068–1072, doi:10.1126/science.1237317.

Wiseman, S. M., R. E. Arvidson, R. V. Morris, F. Poulet, J. C. Andrews-Hanna, J. L. Bishop, S. L. Murchie, F. P. Seelos, D. Des Marais, and J. L. Griffes (2010), Spectral and stratigraphic mapping of hydrated sulfate and phyllosilicate-bearing deposits in northern Sinus Meridiani, Mars, *J. Geophys. Res.*, *115*, E00D18, doi:10.1029/2009JE003354.

Wray, J. J. (2013), Gale Crater: The Mars Science Laboratory/Curiosity rover landing site, *Int. J. Astrobio.*, *12*, 25–38, doi:10.1017/S1473550412000328.